AD-A051 051 ARMY ARMAMENT RESEARCH AND DEVELOPMENT COMMAND ABERD--ETC F/G 7/4
ENERGY TRANSFER IN A2 SIGMA OH. I. ROTATIONAL.(U)
JAN 78 R K LENGEL, D R CROSLEY

UNCLASSIFIED ARBRL-TR-02035 NL

| OF |
AD
A051051

END
DATE
FILMED
4-78
DDC

BRL

AD

(12)

TECHNICAL REPORT ARBRL-TR-02035

ENERGY TRANSFER IN $A^2\Sigma$ OH

I. ROTATIONAL

Russell K. Lengel
David R. Crosley

January 1978

Approved for public release; distribution unlimited.

USA ARMAMENT RESEARCH AND DEVELOPMENT COMMAND
USA BALLISTIC RESEARCH LABORATORY
ABERDEEN PROVING GROUND, MARYLAND

Destroy this report when it is no longer needed.
Do not return it to the originator.

Secondary distribution of this report by originating or sponsoring activity is prohibited.

Additional copies of this report may be obtained from the National Technical Information Service, U.S. Department of Commerce, Springfield, Virginia 22161.

The findings in this report are not to be construed as an official Department of the Army position, unless so designated by other authorized documents.

The use of trade names or manufacturers' names in this report does not constitute indorsement of any commercial product.

UNCLASSIFIED

SECURITY CLASSIFICATION OF THIS PAGE (When Data Entered)

REPORT DOCUMENTATION PAGE	READ INSTRUCTIONS BEFORE COMPLETING FORM
1. REPORT NUMBER: TECHNICAL REPORT ARBRL-TR-02035	2. GOVT ACCESSION NO.
3. RECIPIENT'S CATALOG NUMBER	
4. TITLE (and Subtitle): ENERGY TRANSFER IN A $^2\Sigma^+$ OH I. ROTATIONAL	5. TYPE OF REPORT & PERIOD COVERED: Technical rept.
6. PERFORMING ORG. REPORT NUMBER	
7. AUTHOR(s): Russell K. Lengel* [redacted] David R. Crosley	8. CONTRACT OR GRANT NUMBER(s)
9. PERFORMING ORGANIZATION NAME AND ADDRESS: US Army Ballistic Research Laboratory, Aberdeen Proving Ground, MD 21005	10. PROGRAM ELEMENT, PROJECT, TASK AREA & WORK UNIT NUMBERS: RDT&E 1L161102AH43
11. CONTROLLING OFFICE NAME AND ADDRESS: US Army Materiel Development & Readiness Command, 5001 Eisenhower Avenue, Alexandria, VA 22333	12. REPORT DATE: JAN [redacted] 78
	13. NUMBER OF PAGES: ~~59~~ 58 pp
14. MONITORING AGENCY NAME & ADDRESS (if different from Controlling Office)	15. SECURITY CLASS. (of this report): Unclassified
	15a. DECLASSIFICATION/DOWNGRADING SCHEDULE

16. DISTRIBUTION STATEMENT (of this Report)

Approved for public release; distribution unlimited.

17. DISTRIBUTION STATEMENT (of the abstract entered in Block 20, if different from Report)

18. SUPPLEMENTARY NOTES

*Department of Chemistry, University of Wisconsin

19. KEY WORDS (Continue on reverse side if necessary and identify by block number)

Energy Transfer
Rotational Relaxation
OH Molecule
State-to=state Transfer
Laser Excited Fluorescence

20. ABSTRACT (Continue on reverse side if necessary and identify by block number)

We have used a frequency doubled, tunable dye laser (real) is used to excite individual v, N, J levels of the A-state of the OH molecule. The fluorescence emitted in the presence of known pressures of various fill gases has permitted the determination of collisionally-induced population changes, and hence state-to-state energy transfer rates. Here are reported results on rotational energy transfer within v = 0, using six different initially pumped levels for nitrogen as a collision partner, and two each for hydrogen and argon. It is found that the

(over)

DD FORM 1 JAN 73 1473 EDITION OF 1 NOV 65 IS OBSOLETE

393471

UNCLASSIFIED

SECURITY CLASSIFICATION OF THIS PAGE (When Data Entered)

Item 21. (Contd)

rates are fast (14 per torr per microsecond for a typical total transfer rate with nitrogen), that a process having $\Delta N = \Delta J$ occurs faster than one where $\Delta N \neq \Delta J$, and that multiquantum transfer rates are nearly as large as single quantum transfer rates.

Delta

Delta

not equal

TABLE OF CONTENTS

LIST OF ILLUSTRATIONS

LIST OF TABLES

INTRODUCTION

A convincing argument can be made that the purpose of physical chemistry is the complete understanding of a reaction

$$A + B \rightarrow C + D$$

where A, B, C, and D are particles of chemical interest, such as atoms, molecules, ions, or photons. Much effort, both experimental and theoretical, has been expended on the elucidation of the properties of the isolated components of the reaction - naturally of fundamental importance to its description - and very detailed information is available about these properties. Most reactions have been studied primarily by bulk experiments in which an ensemble of A molecules at some temperature T is mixed with a similar ensemble of B, and the temperature and composition of the mixture measured either after equilibrium has been established or as a function of time. Now, however, specific examples are beginning to be studied, both experimentally and theoretically,[1] at the level of single encounters of molecules in pure quantum states. That is, the question now being addressed is that of the probability, given a molecule of A in internal quantum state i passing by molecule B in state j with velocity $\vec{v}$ and at a distance b, that a reaction will occur to give molecule C in state k and D in state m with velocity $\vec{v}_C$ and $\vec{v}_D$. This probability, $p(A,i,B,j,\vec{v},b,C,k,\vec{v}_C,D,m,\vec{v}_D)$, is the most detailed information that can be obtained about the system, and all less detailed information, such as bulk rates or thermodynamic properties, can be obtained by appropriate statistical averaging. It is, of course, unfeasible to study even all simple reactions on a state specific basis, and it is usually more efficient and accurate to obtain bulk results by direct measurements than by statistically averaging detailed information. Rather, it is to be hoped that the understanding gained from detailed studies of a few reactions will allow fundamental interpretations and deconvolutions to be made from the much larger body of bulk properties, and will indicate those applications in which these bulk properties can be adequately used and those in which detailed information is required.

The many possible (separately measurable) outcomes from such an encounter may be conveniently divided into three physically distinct categories: molecule A may simply suffer a change in its velocity $\vec{v}_A$ in an elastic collision; the internal quantum state of one or both of the particles may be changed in an energy transfer collision (the term energy transfer is used here somewhat loosely to include transitions between degenerate internal quantum states, such as the z components of angular momenta); or the molecules may be converted to chemically different species in a reactive collision. It is conceptually possible to

[1] R. N. Zare and P. J. Dagdigian, "Tunable Laser Fluorescence Method for Product State Analysis," Science 185, 739-747 (1974).

study all three processes with a single experiment or theoretical formalism, but of practical necessity they are generally investigated separately; a limit on the specificity attainable is dictated by what may be considered as a fundamental law of experimental chemical dynamics: information is gained only through a loss of signal. In this series of energy transfer experiments, it has been possible to determine the rate at which the OH molecule, in a specific vibrational (v), rotational (N), and total angular momentum (J) state of the excited $A^2\Sigma^+$ electronic state, will undergo transitions, induced by collisions with a fill gas at a given pressure, that change one or more of the quantum numbers by a given amount. That is, the set of reactions studied is

$$OH(A^2\Sigma^+, v_i, N_i, J_i) + M \rightarrow OH(A^2\Sigma^+, v_f, N_f, J_f) + M$$

where M represents the colliding fill gas. The initial state of the OH molecule is selected by laser excitation, and the final states resulting from the collision are determined by dispersion of the ensuing fluorescent emission. The use of a tunable laser permits variation of the initial state of the OH, so that an array of rates specific to both initial and final states can be extracted. On the other hand, the states of the collision partner M (which is He, Ar, H_2, D_2, or N_2) are not specified: its initial state distribution is that of a thermal ensemble at a known temperature, and its final state distribution cannot be probed. This is thus still far from the ultimate level of detail, but the ability to probe a range of both initial and final states of one of the collision partners has been sufficient to show a number of interesting and important trends. Among these is the direct observation[2] of a new effect, *viz.* the rotational level dependence of a highly exoergic vibrational transfer rate - hitherto generally ignored but with noticeable consequences for interpretation of bulk experiments as well as for development of theories of collision dynamics.

The choice of the hydroxyl molecule, and the set of variables studied, comes from considerations, not necessarily in order, of theoretical tenability and utility, practical importance, and experimental convenience. The theoretical importance of OH is due to its size or, more explicitly, its number of electrons, nine. Only recently have *ab initio* calculations yielded good enough wavefunctions for the OH molecule to accurately predict such properties as the dipole moment[3] of the A state and relative electronic transition probabilities[4] of the A-X system. When it is realized that not only the properties of the OH, but also those of the collision partner and the interactions between the two molecules are

---

[2] R. K. Lengel and D. R. Crosley, "Rotational Dependence of Vibrational Relaxation in $A^2\Sigma^+$ OH," Chem. Phys. Lett. 32, 261-264 (1975).

[3] S. Green, "Dipole Moment and Hyperfine Constants of OD $A^2\Sigma^+$ from ab initio Calculations," J. Chem. Phys. 58, 4327-4330 (1973).

[4] W. H. Henneker and H. E. Popkie, "Theoretical Electronic Transition Probabilities in Diatomic Molecules. I. Hydrides," J. Chem. Phys. 54, 1763-1778 (1971); B. Liu, "Accurate Theoretical Oscillator Strengths for Diatomic Molecules, CH and OH," Symposium on Molecular Structure and Spectroscopy, Columbus, Ohio, June 1975, Paper RF 14.

necessary to theoretically model the collision process, the need for simplicity is obvious. Of the ten molecules that are simpler than OH (six hydrides and four homonuclear diatomics), detailed energy transfer results are available for only two, Li_2 and H_2. The results obtained here for collisions of OH with H_2 and D_2 are quite detailed and reliable, providing important input parameters for semiempirical calculations and comparison values for *ab initio* calculations* that might be done for these simple systems. Even though the N_2 molecule presents considerable theoretical complications as a collision partner, there are evident important effects and trends that must be accounted for and treated explicitly in approximate calculations.

There are two areas of practical importance that require detailed energy transfer rates. The first of these is laser studies. The A-X system of OH has been proposed[5] as a laser candidate; moreover, the results presented here provide information of general applicability to laser design. For all lasers in general and gas phase chemical lasers in particular, the prime loss mechanism of the upper level, except for the laser emission itself, is energy transfer. The results presented here add to this understanding as a test of transfer models that might be used in laser characterizations especially with regard to insights into energy transfer processes undergone by the hydrogen halides, which are physically similar to OH and are important chemical laser molecules.

The second area, to which these results are of direct applicability, is the understanding of modelling of complicated reaction networks. There is increasing evidence that many reactions, both chemical and photochemical, give rise to products with a wide variety of non-thermal internal state distributions, and that the influence of internal energy on reaction rates can differ greatly from that predicted by simple activation energy concepts.[1,6] It is then necessary to use state to state reaction rates as well as detailed energy transfer rates in such models. There are three such networks under currently intense investigation which include OH as a major constituent.

The first of these is that involving combustion processes. The oxidation of any hydrogen containing fuel produces the OH molecule in both the ground and excited electronic states. The rates of initial production of the radical and the rates of its subsequent reactions, along with various reformation reactions, are critically important in the overall combustion process. Besides its importance as a key intermediate

*For a vibrational energy transfer collision of OH in v'=1, N'=0 with H_2 in a thermal distribution near 300K, a total of 11 electrons and 22 internal energy levels must be considered.

[5]C. H. Chen and M. G. Payne, "A Potential Hydroxyl Ultraviolet Laser," Opt. Comm. 18, 476-478 (1976).

[6]M. J. Berry, "Laser Studies of Gas Phase Chemical Reaction Dynamics," Ann. Rev. Phys. Chem. 26, 259-280 (1975); J. H. Birely and J. L. Lyman, "Effect of Vibrational Reagent Energy on Measured Reaction Rate Constants," J. Photochem. 4, 269-280 (1975).

species, OH is relatively easily and widely probed spectroscopically. Understanding and unraveling the details of combustion processes, whether to increase efficiency or to reduce the production of pollutants, requires the use of models including energy transfer rates of the OH.

The second and third networks concern the chemistry of two levels of the atmosphere. Investigations of the biologically important troposphere are aimed primarily at deducing the effects of man-made pollutants, mainly hydrocarbons, oxides of nitrogen, and carbon monoxide. As Levy states,[7] "The driving force behind tropospheric photochemistry is OH ...". Models and understanding necessary to eliminate photochemical smog require a detailed understanding of OH reaction rates. In the stratosphere a very complex network of reactions is required to explain the natural abundance of the molecules of interest as well as the perturbations caused by artificially introduced species;[8] many of these reactions contain OH as either a product or reactant. Here, due to the low pressures and to the number of reactions that lead to highly excited products, it is especially imperative to use state to state reaction and energy transfer rates for adequate models of stratospheric chemistry.

These considerations, and the fact that OH is a nearly ubiquitous and relatively stable free radical, have made it the subject of many and varied examinations. While, as is often the case, well studied is not necessarily synonomous with well determined, the abundance of previous investigations of OH make it a particularly convenient molecule for study. Bulk reaction studies provide prescriptions for its production,[9] while the monumental spectroscopic investigation of Dieke and Crosswhite[10] is an indispensable precursor to this work. Finally, the location of the A-X absorption bands is within the wavelength range of presently available frequency doubled dye lasers, while both the absorption and emission lines show a coarse rotational structure with little overlapping of different vibrational bands. With the aid of the Dieke and Crosswhite study, a wide range of initial and final states can be cleanly and reliably chosen and detected.

---

[7] H. Levy, "Photochemistry of the Troposphere," Adv. Photochem. 9, 369-524 (1974).

[8] M. Nicolet, "An Overview of Aeronomic Processes in the Stratosphere and Mesosphere," Can. J. Chem. 52, 1381-1396 (1974).

[9] F. Kaufman and F. P. Del Greco, "Formation, Lifetime and Decay of OH Radicals in Discharge Flow Systems," J. Chem. Phys. 35, 1895 (1961).

[10] G. H. Dieke and H. M. Crosswhite, "The Ultraviolet Bands of OH," John Hopkins University Bumblebee Report No. 87 (1948), republished in J. Quant. Spectry. Radiat. Transfer 2, 97-199 (1962).

Our studies of the energy transfer within the $A^2\Sigma^+$ state of OH will be presented in three parts. This, the first, deals with rotational energy transfer within v' = 0 in OH. The second[11] treats vibrational energy transfer from v' = 1 and v' = 2 in OH and OD, elucidating upon a physical picture of the collision process involving relatively long-lived collisions. The third part[12] is concerned with an analysis of the data using information theoretic techniques,[13] some results of which may be incorporated into the data analysis as well as providing further support for the physical picture developed in II. Experimental details are presented in this portion, with the exception of a few aspects pertinent only to the vibrational transfer, plus corrections to the simplified steady state approximation used throughout; these last topics appear in II. Further details and amplification may be found in the thesis[14] of one of the authors (RKL), from which much of this series is taken.

EXPERIMENTAL DETAILS

The experimental realization of the goals outlined above is accomplished by the utilization of selective excitation spectroscopy as shown pictorially in Fig. 1. Molecules of OH in the ground electronic state are excited by photon absorption to a specific vibrational, rotational, and electron spin level of the $A^2\Sigma^+$ state. Unperturbed, these molecules will radiate only certain characteristic lines, with the intensity of each proportional to the population of that level. When perturbed by collisions, the initially excited molecules can undergo vibrational or rotational (see inset) transfer to other levels in the A state, the identity and population of which can be determined from the ensuing fluorescence, or can lose electronic energy in a quenching collision. The apparatus used to accomplish this is shown in the block diagram of Fig. 2 and is divided into three parts: the flow system for the production of the OH and the addition of collision partners; the laser system used to excite the molecules; and the monochromator and electronics necessary to quantitatively detect the fluorescence.

---

[11] R. K. Lengel and D. R. Crosley, Energy Transfer in $A^2\Sigma^+$ OH. II. Vibrational," to be published (referred to as II).

[12] R. K. Lengel and D. R. Crosley, "Energy Transfer in $A^2\Sigma^+$ OH. III. Surprisal Analysis," to be published (referred to as III).

[13] R. D. Levine and R. B. Bernstein, "Energy Disposal and Energy Consumption in Elementary Chemical Reactions: the Information Theoretic Approach," Acct. Chem. Res. 7, 393-400 (1974).

[14] R. K. Lengel, "Energy Transfer in $A^2\Sigma$ OH," Ph.D. Thesis, University of Wisconsin, Madison, WI, June 1976.

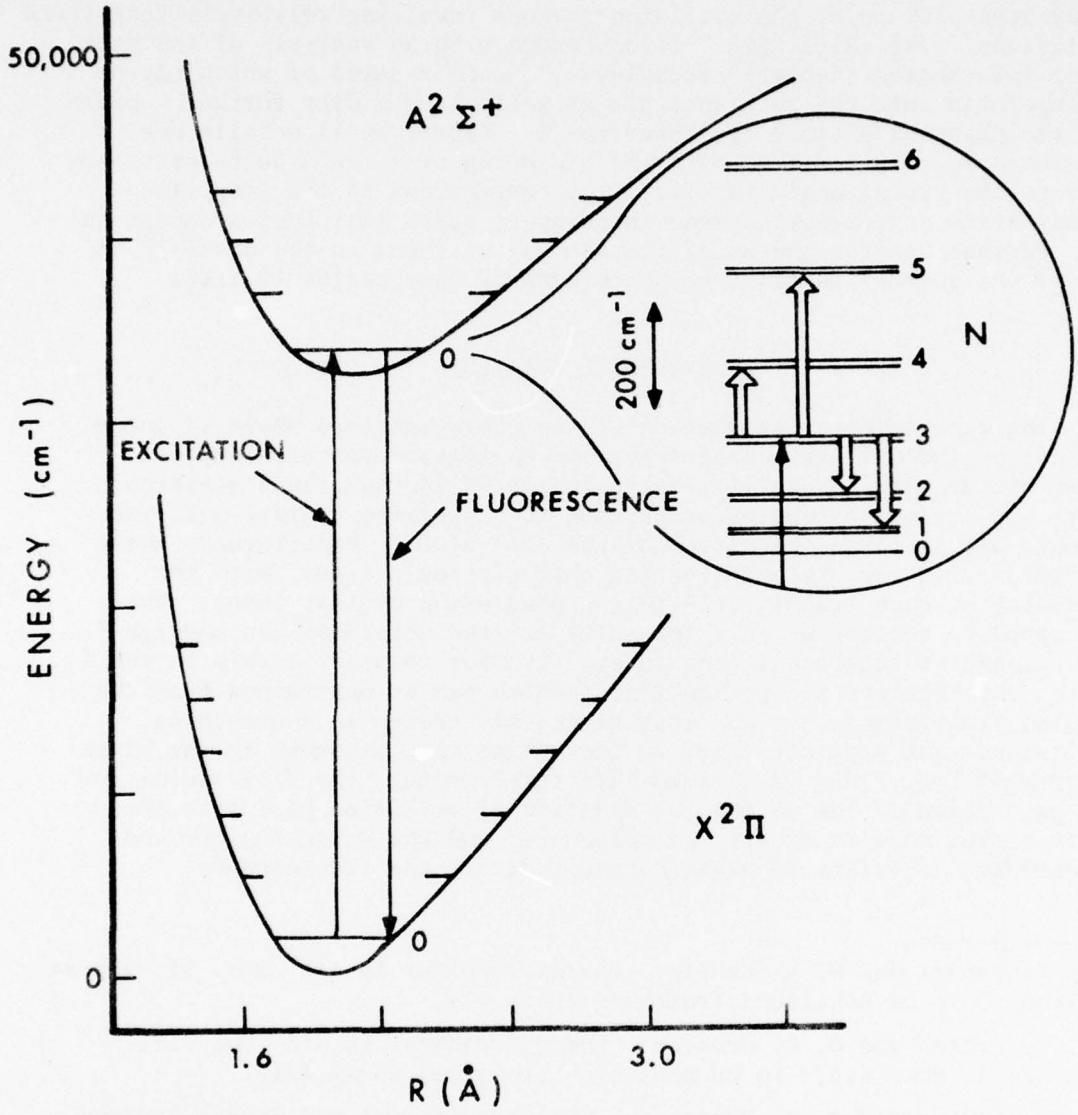

Figure 1. Potential energy curves, and energy levels, for the A and X states of OH probed by selective excitation of fluorescence. The inset shows the lower lying rotational levels, with $F_1(3)$ pumped by the laser. A few collisionally induced transitions are denoted by heavy arrows.

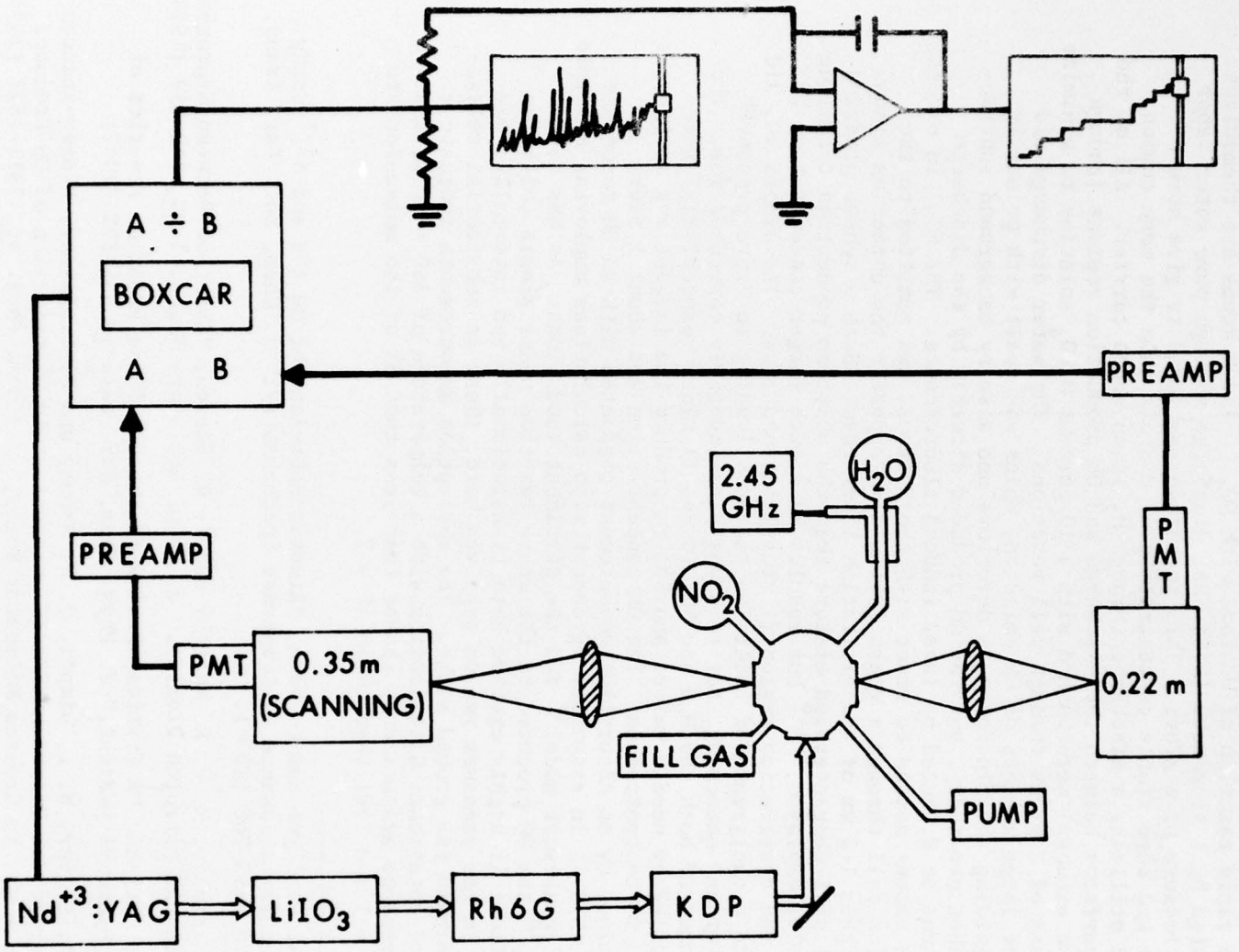

Figure 2. Experimental set-up. See text for description. The second recorder, which exhibits the integral of the intensity as a function of wavelength, is used only in the measurements of vibrational transfer (see II).

The OH is continuously produced in a fast (3ℓ sec^{-1}) flow system by the rapid reaction of H atoms with NO_2.[9] The H atoms are themselves generated by a microwave (2.54 GHz) discharge through pure water vapor at a pressure of 6 mTorr. This technique was found to give here a larger and more stable concentration of H atoms than the more common method utilizing a discharge through H_2 in an argon carrier. All of the cell surfaces between the discharge and OH production regions (though not the windows) were washed with a 10 percent H_3PO_4 solution to minimize the loss of H atoms through wall reactions.[3] The water discharge did produce large amounts of OH emission, which was dealt with primarily by shielding the fluorescence detectors and also by background subtraction when necessary, but the OH produced directly by the discharge could not be detected by laser induced fluorescence. The NO_2, in excess of the amount needed to react with the H atoms, was admitted[2] to the reaction cell through a glass frit placed opposite the detection window and within 1-2 mm of the excitation laser beam. Such a scheme produced a less well characterized mixture than the upstream production technique generally employed,[15,16] but results in a much larger concentration of OH in the observation region (1 mTorr) in this case. The excess NO_2 did produce a background of collision partners leading to "zero pressure" transfer and quenching, but this was experimentally corrected for. The pressures of both the H_2O and NO_2 (6 and 11 mTorr respectively) were controlled by needle valves and set to produce the largest and most stable OH concentration. The OH concentration was about 1 mTorr, as determined by an absorption measurement conducted with an OH resonance lamp; this is in essential agreement with calculations employing a simple reaction network model[17] and the pertinent conditions. As has been shown,[18] the OH produced by the above reaction under single collision conditions is highly excited both translationally and internally; however, in the pressure region employed here, there is substantial relaxation within the ground state. The absorption measurements indicate a thermal rotational distribution with a temperature of 360 ± 60°K, and fluorescence measurements showed that less than 5% of the molecules are in v" = 1 and less than 1% in v" = 2.

---

[15] M. A. A. Clyne and S. Down, "Kinetic Behaviour of OH $X^2\Pi$ and $A^2\Sigma^+$ Using Molecular Resonance Fluorescence Spectrometry," J. Chem. Soc. Far. Trans. II 70, 253-266 (1974).

[16] A. McKinzie, M. F. R. Mulcahy and J. R. Steven, "Reaction Between Hydrogen Atoms and Nitrogen Dioxide," J. Chem. Soc. Far. Trans. I 70, 549-559 (1974).

[17] W. E. Wilson, "A Critical Review of the Gas-Phase Reaction Kinetics of the Hydroxyl Radical," J. Phys. Chem. Ref. Data 1, 535-572 (1972).

[18] J. A. Silver, W. L. Dimpfl, J. H. Brophy and J. L. Kinsey, "Laser-induced Fluorescence Determination of Internal-state Distribution of OH Produced by H + NO_2 in Crossed Molecular Beams," J. Chem. Phys. 65, 1811-1822 (1976); H. Haberland, P. Rowher and K. S. Schmidt, "Reactive Scattering of H and D Atoms. II. Isotope Effect on the Angular Distribution of H,D and NO_2," Chem. Phys. 5, 298-305 (1974); J. C. Polanyi and J. J. Sloan, "Detailed Rate Constants for the Reactions Atomic Hydrogen + Ozone → Hydroxyl (v'J') + Molecular Oxygen, and Atomic Hydrogen + Nitrogen Dioxide → Hydroxyl (v'J') + Nitrogen Monoxide," Int. J. Chem. Kinet. 7, (Symp 1), 51-60 (1975).

The fill gases or collision partners used here (Ar, H_2, and N_2) were admitted to the cell directly from tanks through a shower-head located 10 cm from the observation region and pointing upstream to the gas flow to assure uniform mixing. The pressures were controlled by means of needle valves and measured with an alphatron gauge located downstream of the observation region. The alphatron gauge was calibrated against a McLeod gauge for each of the gases and pressure ranges involved. Both calculations, using the pumping speed of the system and the dimensions of the cell, and experimental observations, using a cell with dimensions similar to the OH production cell but with several inlet and pressure measuring ports, showed that no detectable error is introduced by this method.

One final feature of the flow system, not directly concerned with OH production but important nonetheless, was the use of a stainless steel cold trap to protect the mechanical pump from condensible vapors. In the glass trap originally used, frequent and often violent explosions occured even though it was immersed in liquid N_2. The stainless steel walls apparently caused a catalytic destruction of the labile species, similar in effect to the silver gauze used in the one other report[16] of this phenomenon, and prevented further detonations.

The laser used to excite the OH was a commercial system (Chromatix) consisting of a flashlamp pumped Nd^{+3}:YAG laser with intracavity doubling; this is used to pump a tunable dye laser whose doubled output falls in the OH absorption region. The YAG laser was operated in the Q-switched mode to produce 180 nsec pulses of 3 KW peak power at 75 pps. The doubled output of the dye laser, using Rh6G, had 50 W of peak power, a beam area of 0.02 cm^2 at the cell inlet window and a full width at half maximum (FWHM) of ~ 6 cm^{-1}. The shape and width of the uv laser pulse was indistinguishable (within 20 nsec) from that of the dye fundamental, which had a width of 100 nsec. The laser beam was directed to the cell and its position controlled by two mirrors. An exit window and third mirror provided for two-pass excitation of the OH.

For the rotational transfer experiments described here, all excitations and observations were confined to the 0,0 band of the OH (3060-3120 Å). The levels studied, $N' = J' - 1/2 = 0$, 1, 3, and 4, were produced with $P_1(N'+1)$ excitations (the rotational branch notation is that of Dieke and Crosswhite, ref. 10) to overcome the laser bandwidth limitation (which is larger than the A state doublet splitting) via the rigorous selection rule $\Delta J = 0, 1$. The $N' = 0$ level was excited with the $P_2 1'$ branch, due to the overlap of the $P_1 1$ with the $Q_1 3$ line, and the $N' = 6$ level was excited with the $Q_1 6$ line due to the low population in $N' = 7$ (here the small line strength of the $Q_1 6'$ satellite insures that predominately $J' = 6'$ is excited).

As with any spectroscopic investigation, the detection apparatus is the central part of the experiment. The light emitted by the initially excited and collisionally populated levels is collected by a quartz lens and focused on the entrance slit of a 0.35 m scanning monochromator. The use of a 1200g/mm grating blazed at 5000 Å in the second order with 50 micron slits gave a final bandwidth (FWHM) of 0.75 Å. This is considerably wider than the Doppler broadened OH emission so that the population of any level is directly proportional to either the peak height or area of each of its individual emission lines. This resolution was not sufficient to fully separate the OH emission into these individual lines, but enough information was obtained to assign populations to all N', J' levels. The dispersed radiation was detected with an EMI 6256S photomultiplier (PMT). The response of the monochromator-detector system as a function of wavelength was determined previously[19] and found to be flat over the wavelength region of interest here.

The photocurrents from the PMT were preamplified by a small current to voltage transducer built around an AD507 operational amplifier. This device was relatively slow, having a fall time of 23 μsec as compared to the signal fall times of less than 1 μsec, but this response was advantageous in terms of stability (i.e. freedom from oscillation and pulse ringing), low noise (smoothing out the PMT shot noise and rejecting the RF noise produced by the laser), and the ability to use simple steady state formalism to describe its signals (see appendix to II). The final processing of the signals was done with a PAR model 162 boxcar averager with type 164 gated integrator plug-ins. The boxcar, triggered by the Q-switch synchronization pulse of the YAG laser, was operated with a gate width of 13 μsec, and an effective time constant of 1 sec. Since the boxcar had a fixed gain, a precision step attenuator was placed between it and the preamplifier to provide optimum signal levels. That is, the use of the boxcar permitted the low duty cycle pulsed signals, having an average current of 1-3 na, to be read with effective peak currents of 1-3 μa.

The output of the boxcar, the intensity of the OH emission as a function of time (and hence wavelength) when the monochromator was scanned, was displayed on the Y axis of a Hewlett-Packard model 70058 recorder while the X axis was driven by a 17108A time base. As all intensities were taken from this recorder, it was carefully checked for Y axis linearity by the use of a constant voltage source and a calibrated attenuator. The calibration of the wavelength axis was unimportant here as the easily recognized and well located OH lines provided a built in standard when needed. Also shown in Fig. 2 is a recorder displaying the integral of the output signal vs. wavelength; this is used only in the vibrational transfer studies (see II).

---

[19] D. R. Crosley and R. K. Lengel, "Relative Transition Probabilities and the Electronic Transition Moment in the A-X System of OH," J. Quant. Spect. Rad. Transfer 15, 579-591 (1975).

The smaller monochromator shown in Fig. 2 was used in a wide-bandpass mode (~ 100 Å) to collect a large portion of the fluorescence and provide a normalizing signal. Slow drifts in the absolute signal level over an individual run (usually 8 min scan time) were unavoidable, and due primarily to changes in the dye laser wavelength as well as smaller contributions from variations in the laser power output and OH ground state concentrations. Such drifts (generally less than 25%) could be adequately corrected for by the monitoring detector and the analog divider incorporated in the boxcar recorder. Larger changes sometimes occurred, but they were readily recognizable and such scans were discarded.

DATA ANALYSIS

Typical scans of the (0,0) band are shown in Fig. 3. On the left-hand side is the fluorescence obtained when the $F_1(1)$ level is pumped in the absence of a collision partner. It consists predominantly of the five strong branches $Q_1 1$, $Q_2 1'$, $P_1 2$, $P_2 2'$ and $O_2 3$ denoted in the figure. The remaining lines are due to rotational transfer collisions with the background gases; while accounted for in the actual analysis procedure (see appendix), these lines and collisions will be largely ignored in the discussion. The right hand side shows the spectrum emitted by OH, still initially excited to $F_1(1)$, in the presence of 0.86 torr N_2. Many more lines are here evident, due to emission from other rotational levels populated by collisions with the N_2. However, the $F_1(1)$ level still retains an appreciable fraction of the population, well above that existing under a thermal distribution. This is especially evident in the Q_1 series, denoted in the figure. The fractional population in $F_1(1)$ at 0.86 torr N_2 is 23% (see below, Table 1), compared to a 300K Boltzmann distribution fraction of 13%.*

From scans such as those in Fig. 3, taken at several pressures of the collision partner, relaxation rates for collisions between individual rotational levels may be obtained. The extraction of these values - the essential results of this paper - proceeds in two steps, first, obtaining the populations of the appreciably populated rotational levels from the spectral scans, and second, fitting these pressure-dependent populations within a steady-state kinetics treatment to obtain the collisional transfer rates. This section deals with, in turn, the determination of the populations, the idealized kinetic equations used, and other necessary parameters (lifetimes and temperature). The necessary corrections to the idealized (steady-state) kinetic equations used here are dealt with in the appendix to this paper and the appendix to II.

*The fractional population in $F_1(1)$ for the zero-pressure scan is 62%, i.e., the background gas does lead to appreciable transfer.

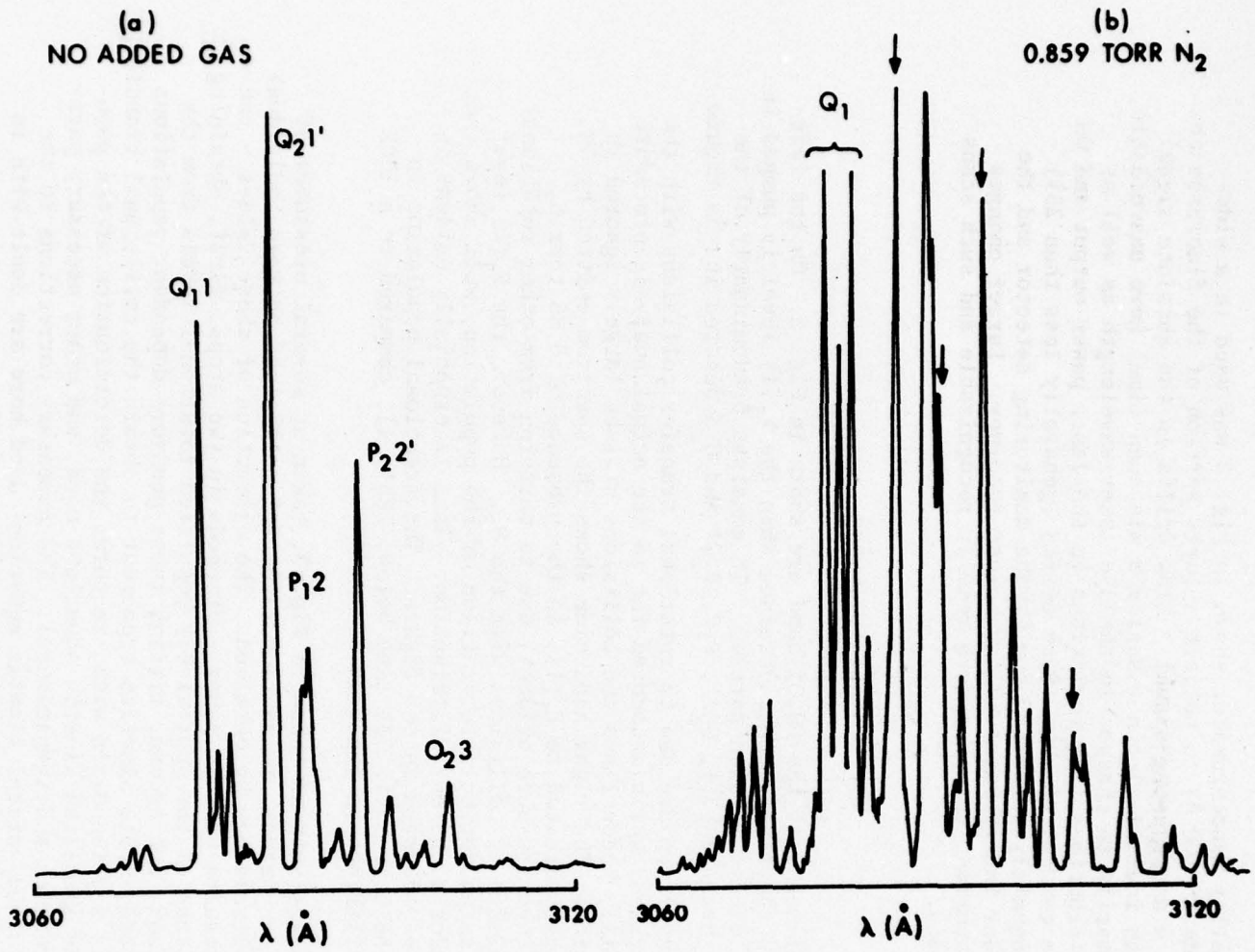

Figure 3. Scans of the (0,0) band, pumping the $F_1(1)$ level via absorption in the $P_1(2)$ line. (a) No added gas. The five rotational branches emitted by $F_1(1)$ are marked. The other lines are due to transfer collisions with the background gases H_2O and NO_3 (see text). Some laser scatter is responsible for the width of the feature in the $P_1(2)$ region. (b) Spectrum in the presence of 0.86 torr N_2. The Q_1 series is marked, as are (with arrows) the remaining four branches noted in (a). The peaks seen here, due to rotational energy transfer collisions with the N_2, form the 32 features from which are extracted the level populations.

TABLE 1. FEATURE INTENSITIES AND LEVEL POPULATIONS FOR TYPICAL SCANS

(i) 0.86 torr N_2

Feature	Observed[a]	Fitted[b]	Difference[b]	Predicted[c]	Difference[c]
1	.38	.35	.03	.42	-.04
2	.73	.79	-.06	.78	-.05
3	1.12	1.05	.07	1.19	-.07
4	1.54	1.56	-.02	1.57	-.03
5	1.82	1.72	.10	1.68	.14
6	.49	.35	.14	.52	-.03
7	.73	.63	.10	.72	.01
8	7.54	7.58	-.04	6.99	.55
9	5.52	5.51	.01	5.30	.22
10	6.98	7.01	-.03	6.83	.15
11	2.67	2.68	-.01	3.05	-.38
12	2.03	2.09	.00	1.93	.10
13	7.73	7.75	-.02	7.80	.07
14	.85	.79	.06	.98	-.13
15	8.33	7.79	.54	8.01	.32
16	6.58	6.55	.03	6.33	.25
17	4.77	4.94	-.17	5.01	-.24
18	1.03	.94	.09	.96	.07
19	1.94	1.88	.06	1.88	.06
20	.44	.40	.04	.45	-.01
21	7.35	7.29	.06	6.73	.62
22	3.68	3.74	-.06	3.65	.03
23	1.73	1.73	.00	1.97	-.24
24	2.36	2.36	.00	2.46	-.10
25	1.58	1.44	.14	1.40	.18
26	1.53	1.60	-.07	1.82	-.24
27	1.15	1.24	-.09	1.58	-.43
28	.43	.63	-.20	.65	-.22
29	.28	.27	.01	.33	-.05
30	.23	.26	-.03	.24	-.01
31	.19	.25	-.06	.29	-.10
32	.20	.23	-.03	.40	-.20

[a] All entries arbitrary units, but with the same normalization.

[b] Fit results from Eq. (1).

[c] Predicted using final transfer rates (see discussion).

TABLE 1. FEATURE INTENSITIES AND LEVEL POPULATIONS FOR TYPICAL SCANS

(ii) No added gas

Feature	Observed	Predicted[d]	Difference[d]
1	.02	.02	.00
2	.08	.06	.02
3	.12	.11	.01
4	.22	.22	.00
5	.32	.32	.00
6	.05	.06	-.01
7	.05	.06	-.01
8	6.28	6.24	.04
9	1.23	1.23	.00
10	1.57	1.54	.03
11	.29	.29	.00
12	.12	.12	.00
13	8.01	8.01	.00
14	.04	.04	.00
15	2.04	1.63	.41
16	2.49	2.70	-.21
17	1.12	1.14	-.02
18	.08	.07	.01
19	.58	.62	-.04
20	.03	.03	.00
21	4.51	4.57	-.06
22	.83	.84	-.01
23	.18	.19	-.01
24	.31	.33	-.02
25	1.06	1.09	-.03
26	.16	.16	.00
27	.12	.12	.00
28	.02	.04	-.02
29	.01	.01	.00
30	.07	.04	.03
31	.02	.02	.00
32	.10	.10	.00

[d]Fit results from Eq. (1).

TABLE 1. FEATURE INTENSITIES AND LEVEL POPULATIONS FOR TYPICAL SCANS

(iii) Populations resulting from fits.

i^e	N_i (0.86 torr)	N_i (no added gas)
1	.066	.059
2	.066	.054
3	.226	.631
4	.081	.064
5	.132	.086
6	.067	.025
7	.107	.042
8	.053	.014
9	.065	.019
10	.025	.012
11	.052	.088
12	.023	.004
13	.019	.002
14	.010	.002
15	.009	.001

[e]Level designation as given in text.

Population Determination

Even with the coarse rotational structure of OH, the resolution attainable with the spectrometer used is not capable of providing a spectrum completely free from overlapping lines. The assignment of populations to the individual (N,J) levels therefore requires a deconvolution of the measured intensities.

The populations of the individual levels are determined by a fit to the observed fluorescence spectrum. The intensities from at least three good scans are averaged, before fitting, for each of the pressures and pumped levels used. A scan was determined to be "bad" not from the relative intensities or fitted populations, but rather from experimental conditions such as deviations of laser intensity and cell pressures, instrumental drifts, and environmental changes during a scan that could affect the results. For each of the levels N' = 0,1,3, and 4, the intensities of a total of 32 spectral 'features' (definable, reproducible peaks or obvious shoulders) are used to determine 15 populations (N' = 0-7). When N' = 6 is excited, it is found necessary to include the populations of the N' = 8 levels to account for the observed spectra; in this case 34 features are fit to a total of 17 populations. The intensity at any wavelength of the recorded spectrum can be expressed as

$$I(\lambda) = \sum_{i,\ell} N_i S_{i,\ell} f(\lambda - \lambda_\ell) \qquad (1)$$

where N_i is the population of the i^{th} level, labeled as described below, $S_{i,\ell}$ is the line strength[10,20] of the ℓth rotational branch of emission from i, and $f(\lambda-\lambda_\ell)$ is the fraction of light emitted by this branch, with center at λ_ℓ, that is passed by the monochromator at wavelength λ. This triangular bandpass function* is given by a fullwidth at half maximum of 0.75Å. This truncates the sum to one term in the sparse regions of the spectrum and a maximum of ten terms in the congested Q_2 head region. The wavelengths of the chosen features are not measured,[10] but rather calculated using the known transition frequencies and *estimated* populations - for most features, the wavelength is simply that of its strongest component, although in some cases there is no dominant transition and an average value must be assigned. (Some subsequent adjustments are occasionally found necessary to correct for poor initial estimates of the populations.)

---

[20] L. Klein, "Strengths of the Rotational Lines of OH ($A^2\Sigma$ - $X^2\Pi$) and Occupation of the Molecular Energy Levels in Arc Plasmas," J. Quant. Spect. Rad. Transfer 13, 581 (1973).

* Equal entrance and exit slits are employed.

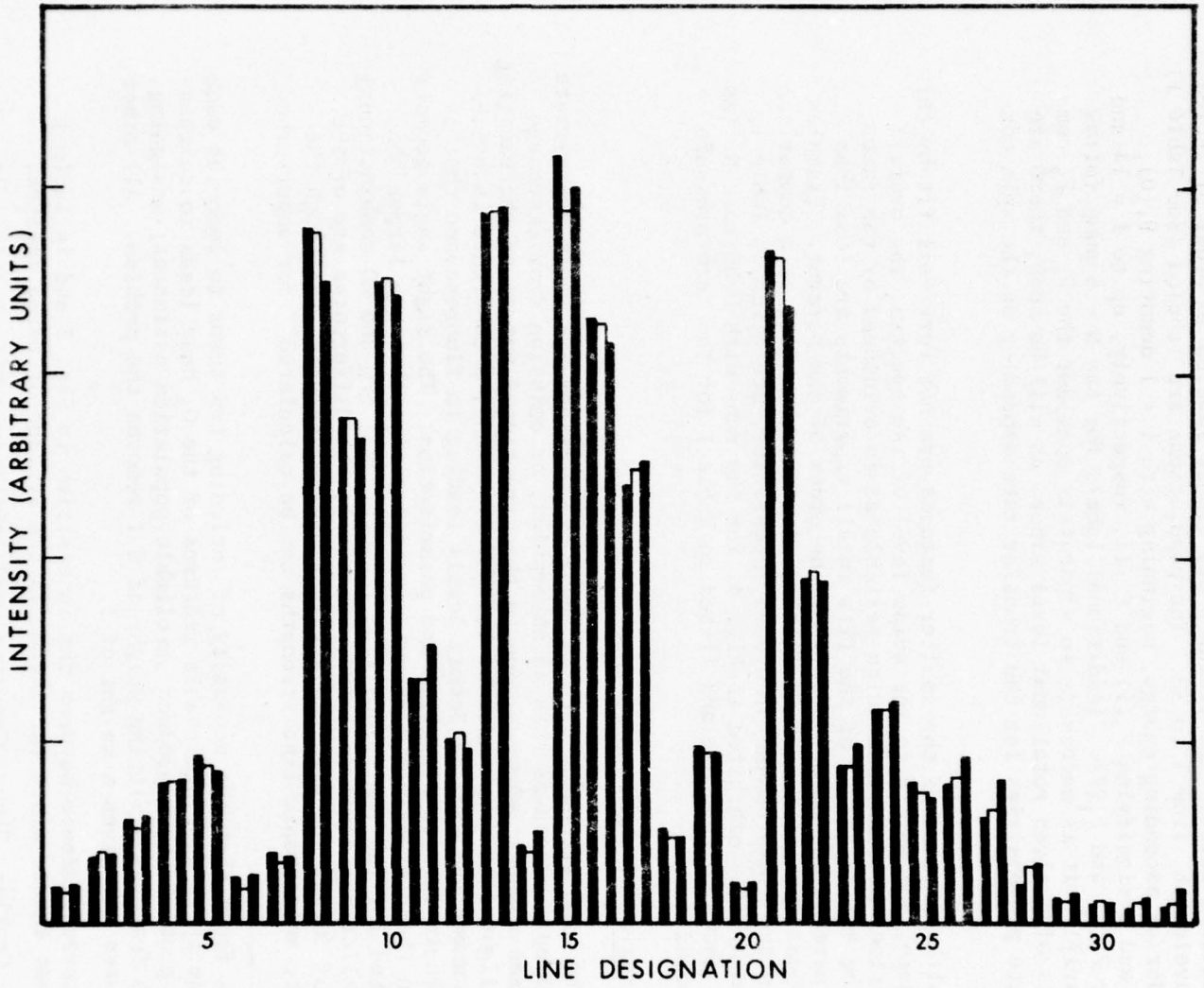

Figure 4. Measured and predicted feature intensities, for N_2 at 0.86 torr. For each of the 32 lines are shown three bars. The left-most (filled) is the measured intensity, the middle (open) is the intensity predicted from the population fit, and on the right (filled) is the intensity predicted using the rate coefficient matrix given in Table 4. The normalization is such that the sum of all intensities for a given category is the same value.

The (overdetermined) system is least squares fitted to the matrix form of Eq. (1), $\vec{I} = \underline{F}\,\vec{N}$, where $\underline{F}$ is the matrix of the factors describing for each feature* the line strengths, line separations, and spectrometer bandpass. The polarizations of the lines must be accounted for separately as described below. The features are simply labeled in order of increasing wavelength, from 1 to 32. The populations are labeled (see Table 1) in order of ascending energy, beginning with i = 1 denoting $F_1(0)$, i = 2 and 3 signifying $F_2(1)$ and $F_1(1)$, respectively, up to i = 14 and 15 for $F_2(7)$ and $F_1(7)$. (Additional labels for the N = 6 pump follow similarly). It is necessary to separately consider the F_1 and F_2 components of a given rotational level since, as will be seen, there are definite propensities for the transfer rate depending on the spin component.

Although some of the smaller features are not very well fit by this procedure, due mainly to the noise level of the spectra, the overall populations produced are quite reliable as is evidenced by the fact that the RMS residuals of the fits in all experiments are less than three percent and more commonly of the order of one percent. Examples of typical results from this fitting procedure, as well as a comparison between the measured and predicted intensities, are given in Table 1, and graphically exhibited in Fig. 4, for the runs with 0.86 torr N_2 (as also** shown in Fig. 3), and listed in Table 1 for the zero pressure background run.

Polarization of the Fluorescence

The line strengths used in these calculations are those appropriate to isotropic processes such as absorption, or emission from discharge and flame sources; whereas, due to the directional nature of the exciting laser light (and compounded by its polarization), a coherence is established among the excited Zeeman levels leading to fluorescence that is anisotropic in both direction and polarization. The right angle geometry used in these experiments results in intensities that are larger than predicted for $|\Delta J \text{ (emission)}| \neq |\Delta J \text{ (absorption)}|$ (PQ and RQ combinations) and smaller for equal $|\Delta J|$ (PR, PP, etc.); the differences are of the order of 30-50% and preclude straightforward analysis.[21] Although the correct, anisotropic line strengths can be calculated[21] for unperturbed

---

*It is found that the necessity of including ten terms to describe each of the three distinguishable features of the Q_2 head leads to correlation problems that produce unreliable population estimates; assigning these features a fitting weight of 0.1 removes the problem. All other features are given a weight of 1.

**The correspondence between the intensities in Fig. 3 and in Table 1 is not exact, since the latter is the average of three spectra.

[21] D. R. Crosley, "Level Crossings and Anisotropic Emission in a $^2\Sigma$ - $^2\Pi$ Transition," BRL Report, to be published.

molecules, the effects of collisional depolarization, stray magnetic fields, and the possibility of retention of coherence[22] upon rotational transfer make such transition probabilities unreliable for the current purpose. Magnetic depolarization (Hanle effect) of the fluorescence is used instead for these experiments. When a magnetic field is applied perpendicular to the direction of absorption and emission, the lifting of the degeneracy of the Zeeman levels destroys their coherence, making the fluorescence less anisotropic; at infinite field, the isotropic and anisotropic line strengths approach one another. Due to the large magnetic g-value and the long radiative lifetime (see below) of the A $^2\Sigma^+$ state,[23] only moderate magnetic fields are required for depolarization. Experimentally, the ratio of P line to Q line emission, which shows the largest coherence effects, has been monitored, both with and without polarized detection, as a function of magnetic field. At the highest field obtainable (~ 5 gauss) the ratio equals that predicted by the isotropic line strengths and is independent of the polarization. The lorentzian line shape of the magnetic depolarization shows a residual polarization at this field that ranges from a minimum of 0.1% for the low-N' levels to a maximum of 1% for N' = 6. This latter value is still undetectable within the noise limitations of the fluorescence signal. This field is then used for all the rotational transfer runs.

Steady-State Equations

The analysis of the population distribution as a function of pressure of the collision partner, in order to determine the rate constants for energy transfer, is carried out with equations obtained from a form of the steady state approximation. The approximation is applied to the populations of all levels except the initially pumped level; these are initially unpopulated. The pertinent equation is then

$$\frac{dN_j}{dt} = 0 = N_e T_{ej} P + \sum_{i \neq e} N_i T_{ij} P - N_j \{ 1 + P[Q + \sum_i T_{ji}] \} , \; j \neq e \qquad (2)$$

where e is the label assigned to the initially excited level. The first two terms represent the collisional input to the population N_j from all other levels N_i (N_e is explicitly singled out for convenience), at a

[22] T. A. Caughey and D. R. Crosley, "Coherence Retention During Rotationally Inelastic Collisions of Selectively Excited Diatomic Sulfur," Chem. Phys. 20, 467-475 (1977).

[23] K. R. German, T. H. Bergemann, E. M. Weinstock and R. N. Zare, "Zero-field Level Crossing and Optical Radio-frequency Double Resonance Studies of the $A^2\Sigma^+$ States of OH and OD," J. Chem. Phys. 58, 4304-4318 (1973).

fill gas pressure P and described by the rate constants T_{ij} for the process $i \rightarrow j$. The negative term represents the loss of population from level j, which occurs due to radiative decay, quenching (rate constant Q), and energy transfer due to collisions. The elastic collision rates T_{ij} have not been explicitly deleted but do cancel in the last two terms.

Experiments such as these fall in the class of competition kinetic measurements; that is, the rate of collisional energy transfer is balanced against radiative decay. The radiative lifetime τ forms a natural clock for the system, and it is convenient to set its value to 1 (for all* levels[24]) as the unit of time. Pressures are measured in torr, so that our working units of transfer rates (and quenching rate) are per torr per lifetime. These units presume no additional absolute parameters (such as τ and translational temperature) and may be directly used for purposes of modelling and assessing fluorescence efficiencies. Conversion to absolute rates is considered below.

Now the system is actually not in a steady state: the laser is pulsed, with a pulse width of about $\tau/8$, and the total excited state population decays with a rate constant $(1 + Q)$. The proper description of the system involves solution of the actual time dependent equations. In the experiment, the time-dependent populations themselves are not monitored, but rather the preamplifier (with a time constant of 33τ) integrates the populations over nearly all time, i.e., we measure quantities which are essentially $\int_0^\infty N_j(t)\,dt$ and denoted by S_j. In Appendix I we demonstrate that these fully integrated signals obey the same equations as Eq. (2), for $j \neq e$ and an initial delta function excitation of level e. (Since we always work with ratios of the S_j to the integrated signal S_e, the equation for N_e itself is redundant.)

Two further corrections are necessary even to apply the integrated intensity ratios S_j/S_e. The first, accounting for the facts that the laser pulse is finite, and that we integrate not to t = B but with a time constant of 33τ, can be expressed by simply using an effective radiative lifetime of 1.03τ. These effects are dealt with explicitly for a two-level system in an appendix to II; extension is readily made to the multiple-level system here by recognizing that the actual populations N_j can be expressed as linear combinations of exponentials in time. Also, while collisions with the background gases cause both energy transfer (as is evident from Fig. 3) and quenching, these effects will be ignored in the development in this section. They are discussed in the Appendix II, and in Ref. 14.

---

*The variation of radiative lifetime with N' is negligible here.

[24] D. R. Crosley and R. K. Lengel, "Relative Transition Probabilities in the A-X System of OD," J. Quant. Spect. Radiat. Transfer 17, 59-71 (1977).

Consequently the use of the steady-state equations (for $j \neq e$) yields nearly the correct result for data analysis purposes. These equations are, we feel, conceptually simpler for exhibiting the actual physics involved, and we prefer to present our description of the collisions in these terms throughout this treatment.

Besides the state-to-state rates T_{ij}, it is also desirable to obtain the total transfer rate out of the initially excited level, $\overline{T}_e = \sum_{j \neq e} T_{ej}$. This is obtained by summing Eq. (2) over all final states j to give

$$N_e P \sum_{j \neq e} T_{ej} + P \sum_{j \neq e} \sum_{i \neq e} N_i T_{ij} - (1 + QP) \sum_{j \neq e} N_j - P \sum_{j \neq e} \sum_{i} N_j T_{ji} = 0$$

but the arbitrary labels in the second term may be rearranged to yield

$$\sum_{j \neq e} \sum_{i \neq e} N_i T_{ij} = - \sum_{j \neq e} N_j T_{je} + \sum_{j \neq e} \sum_{i} N_j T_{ji}$$

so that

$$N_e P \overline{T}_e - (1 + QP) \sum_{j \neq e} N_j - P \sum_{j \neq e} T_{je} N_j = 0 \qquad (3)$$

which may be used to determine $\overline{T}_e$.

Examination of these equations shows that the determination of any T_{ej} or $\overline{T}_e$ requires the knowledge of all other T_{ij}'s. The assumption that is usually made (see e.g. Steinfeld[25]) is that at sufficiently low pressures secondary transfer collisions can be ignored. Then, with an experimental determination of $\overline{T}_e$ from (3) and a knowledge of Q, Eq. (2) gives a linear dependence of N_j on pressure that may be used to determine T_{ej}. For OH the large rotational spacings (which militate against large changes in N'), a spin conservation propensity, and the long radiative lifetime (which allows time for many collisions) enhance the multiple collision effects to such an extent that the "sufficiently low pressures" are here experimentally unattainable.

---

[25] J. I. Steinfeld and W. Klemperer, "Energy Transfer Processes in Monochromatically Excited Iodine Molecules. I. Experimental Results," J. Chem. Phys. 42, 3475-3497 (1965).

Determination of Absolute Rates and Cross-sections

A conversion of our measured rates, on a per torr per lifetime basis, to absolute rate constants ($cm^3\ sec^{-1}$) requires knowledge of the actual radiative lifetime τ of the $v' = 0$ level of the $A^2\Sigma^+$ state. In spite of numerous attempts over many years to measure this troublesome parameter, it has not yet fully yielded to an unambiguous determination. Some of the discrepancies can be accounted for by a change in τ with rotational level and others by rotational and vibrational cascading.[26] Nonetheless, there remain two different values, 0.7 and 0.8 μsec, each supported by more than one experiment, and with error bars which do not overlap. In our opinion, the most reliable results should be obtained from the experiments of German[27] and those of Brophy, *et al.*[28] Each of these studies measures the decay time of time-resolved fluorescence from OH excited by a pulsed frequency doubled dye laser at low pressures. The disagreement between these measurements has been satisfyingly removed by a reanalysis of the latter results.[29] We accordingly adopt a value of 0.7 μsec for τ.

While it is well established experimentally, and realistic theoretically, that the lifetime in $v' = 0$ varies with rotational level, the variation is less than 3% over the range of levels studied here[19] and is ignored in the analysis.

The reduction of measured rates also requires a knowledge of the collision partner number density and the relative velocity ($\bar{v}$) of the colliding pair. The number density determination is easily done, since, at the low pressures (~ 1 Torr) of fill gases used, the ideal gas approximation should be quite valid using the room temperature, which is taken to be 300°K. The calculation of the relative velocity is hampered by what could be a lack of thermal equilibrium between the fill gas and the OH molecules. We assume the measured rotational temperature of 360°K to be similar to the translational temperature (although this temperature does not describe the X-state vibrational distribution under our conditions). A "collision temperature" of 320°K is chosen to calculate the relative velocities; this is not truly an average but rather

---

[26] R. K. Lengel and D. R. Crosley, "Comment on 'Electronic Quenching and Vibrational Relaxation of the OH($A^2\Sigma^+$, v'=1) State'," J. Chem. Phys. 64, 3900-3901 (1976).

[27] K. R. German, "Direct Measurement of the Radiative Lifetimes of the $A^2\Sigma^+$ (v=0) States of OH and OD," J. Chem. Phys. 62, 2584 (1975).

[28] J. H. Brophy, J. A. Silver, and J. L. Kinsey, "Direct Measurement of the Radiative Lifetime of the $A^2\Sigma^+$ (v'=0, K'=1, J'=3/2) State of OH and OD," Chem. Phys. Lett. 28, 418-421 (1974).

[29] W. L. Dimpfl, private communication (1976).

a compromise between the assumed fill gas temperature of 300°K and the OH temperature assumed to be in the range $300^{o}K<\theta<360^{o}K$. Since the temperature enters into the velocity and hence cross section calculation as a square root, this uncertainty in temperature produces an overall uncertainty of only three percent.

The manner in which the experiments are carried out further demands an independent determination of the quenching rate constant for the collision partners studied. We use the values which we have obtained for H_2 and N_2 through the effect of quenching on vibrational transfer data.[11] The values are 1.9 $torr^{-1}\ \tau^{-1}$ for H_2 and 0.98 $torr^{-1}\ \tau^{-1}$ for N_2, which have been determined to within ~ 10%. Ar is a poor quencher and Q(Ar) was too small to produce observable effects in the vibrational transfer work; any quenching will be less noticeable for the rotational transfer. An error in Q (for any collision partner) can have an effect on the state-to-state rates, due to the way in which secondary collisions are accounted for. However, as is true for an error in the lifetimes, its predominant effect should be on the total rates $\overline{T}_e$.

RESULTS

The rotational level populations, determined as a function of fill gas pressure as described in the preceding section, may be used to obtain individual state-to-state collisional rates by application of the steady-state equations also presented there. The high density of rotational levels, and the pressure regime in which these measurements are made requires, however, the consideration of multiple collision effects. That is, an initially excited OH molecule often can undergo more than one rotational transfer collision before losing its electronic energy. Thus, determination of a particular state-to-state transfer rate T_{ij}, by the measurement of two populations N_i and N_j, one of which is initially excited, requires knowledge of all other $T_{k\ell}$ to account for the secondary collisions. For the fill gas (N_2) for which the most complete set of data exists, there are such two-state population measurements for only 70 of the 210 important rates T_{ij}, necessitating both assumptions (such as detailed balancing) and iterative solutions. We thus find it useful to analyze the population data in two qualitatively distinct ways, to determine first the total rotational transfer rates out of the initially pumped levels, and subsequently to treat the state-to-state transfer rates.

Total Transfer Rates

Total rotational transfer out of the pumped level will be treated first since it is less hampered by the effects of secondary collisions, and the total rates themselves are needed as parameters and checks in

the determination of the individual rates. Equation (3) is first rewritten in the more convenient form

$$R_e \equiv (1 + QP)\frac{(1 - N_e)}{N_e} = \overline{T}_e P - P \sum_{j \neq e} T_{je} \frac{N_j}{N_e} \quad ; \qquad (4)$$

the total populations are normalized: $\sum_i N_i = 1$.

The first approximation that can be made is ~~that the multiple~~ collision, back-transfer term is small and that a plot of R_e versus P will be sufficiently linear at low pressures to allow a limiting slope to be drawn that will determine $\overline{T}_e$. This was done to arrive at a first estimate of the total transfer rates. Representative plots are shown by the squares in Fig. 5. The amount of curvature seen in this plot shows that the assumption of small back transfer is not valid, but that the limiting slope will not be in great error. The next assumption that can be made is that this secondary transfer can be represented by a weighted average of the individual back-transfer cross sections

$$B_e = \sum_{j \neq e} \frac{T_{je} N_j}{1 - N_e}$$

which is assumed to be pressure independent, so that

$$R_e = P(\overline{T}_e + B_e) - B_e P/N_e \quad . \qquad (5)$$

The data from the experiments with N_2 as a fill gas are fit to this equation using standard regression techniques to give least squares values for the two parameters $(\overline{T}_e + B_e)$ and B_e. There is an obvious problem of correlation of parameters with this model, but the values for $\overline{T}_e$ obtained are in reasonable agreement with those from the limiting slopes. These values of $\overline{T}_e$ may then be used in the determination of the state-to-state transfer rates for N_2 as a collision partner (next section). The individual T_{je} rates determined *there* are used with the measured populations N_j to *calculate* B_e values at each pressure, and a final linear fit is in turn made to

$$R_e + B_e P(1 - 1/N_e) = \overline{T}_e P$$

(circles and fitted line in Fig. 4). It is found that B_e is effectively independent of pressure and small enough so that a ten percent variation in B_e produced only a two percent variation in $\overline{T}_e$. The final values of $\overline{T}_e$ so obtained, for the five initially excited levels undergoing collisions with N_2, are listed in Table 2.

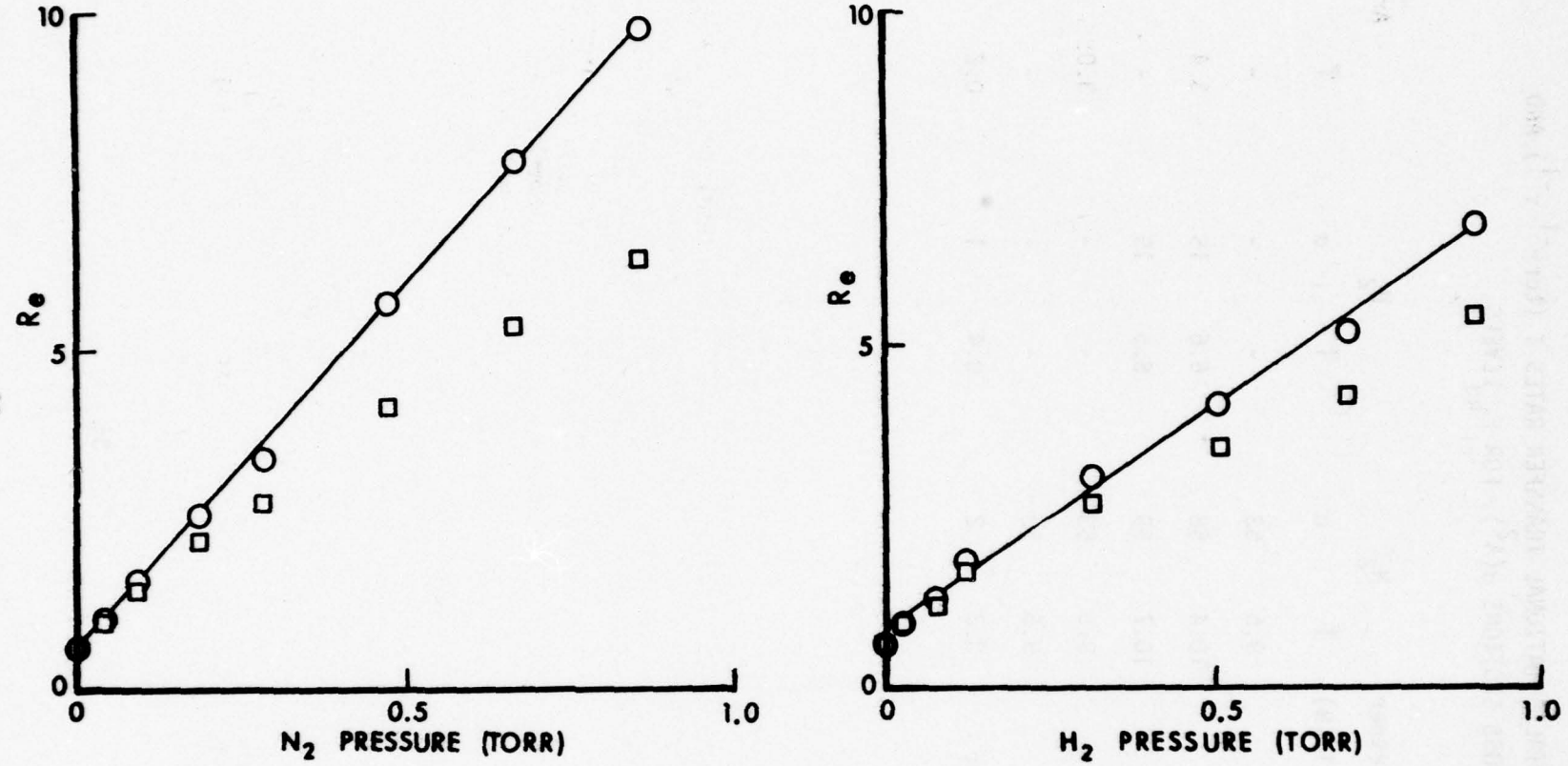

Figure 5. Plots pertinent to total transfer rate determinations. In each case, the $F_1(3)$ level is pumped. The squares are plots of R_e vs. pressure, and the circles represent the values of R_e corrected for back transfer. The points at the two lowest pressures, for both N_2 and H_2, have overlapping squares and circles.

TABLE 2. TOTAL ROTATIONAL TRANSFER RATES $\overline{T}$ ($torr^{-1}\ \tau^{-1}$) AND CROSS SECTIONS $\sigma(Å^2)$, FOR F_1 LEVELS.

Collision Partner	N_2		H_2		Ar	
Excited Level (N)	$\overline{T}$	σ	$\overline{T}$	σ	$\overline{T}$	σ
0	9.5	53	-	-	-	-
1	10.4	58	6.6	15	3.4	20
3	10.7	59	6.5	15	-	-
4	9.5	53	-	-	3.0	18
6	9.5	53	-	-	-	-
Fitting Error	0.3	2	0.4	1	0.2	1

There is not enough data from the work with H_2 and Ar as collision partners to arrive at a reliable B_e from the individual transfer rates, so a ratio method is used. It is assumed that the ratio of the average back-transfer rates B_e in these gases, to $B_e(N_2)$, is the same as the ratio of the total transfer rate $\overline{T}_e$ to $\overline{T}_e(N_2)$. From the limiting slopes, a first estimate of $\overline{T}_e(H_2) = B_e(N_2)\overline{T}_e(H_2)/\overline{T}_e(N_2)$ (and similarly for Ar) is then used to determine new estimates of the $\overline{T}_e$ from linear fits to Eq. (5). Iterative improvement is then used to calculate improved B_e values; convergence is found to occur after five cycles. The final, linearized plot of Eq. (5) for H_2 as a collision partner is also shown in Fig. 5. The same method applied to the Ar data gives similar rapid convergence and straight line plots. The final rates (and cross sections) obtained with all gases and the various initial levels studied are presented in Table 2.

State-to-State Transfer

Before Eq. (2) is used to analyze for the individual, state-to-state transfer rates quantitatively, some qualitative statements about these rates can be made from simple observations of the spectra and the populations obtained from them. The first observation is that, for the levels excited here, only those states with $N' \leq 7$ have appreciable collision induced population, even when the level $N' = 6$ is pumped. This means that the sums in Eq. (2) need be taken only to a value of fifteen. The next observation is that there are no strong propensity rules for $|\Delta N|$ of the transitions; the populations fall off smoothly as $|\Delta N|$ increases and the relative sizes of positive and negative $|\Delta N|$ transitions are in accord with the general notions of energy defect and density of states effects. Finally, it can be seen that there is a propensity for conservation of electron spin upon transfer; in these experiments (where only F_1 levels are excited) it is usually found that $F_1(N')$ has a larger population than $F_2(N')$, even after correction for the degeneracy difference of the two levels.

As before, the steady state equation is first rewritten:

$$R_{ej} \equiv N_j(1 + Q + \overline{T}_j)P/N_e$$

$$= T_{ej}P + B_{ej}P/N_e \qquad (6)$$

where $B_{ej} = \sum_{i \neq e} N_i T_{ij}$.

(Here collisions with the background gases enter intimately into the analysis procedure. They will be ignored here in the spirit of simplification, but see Appendix II for the correct equations.) This equation

immediately shows the problem encountered in the determination of the individual T_{ej}; some method must be used to calculate the term B_{ej}. To illustrate the effect of this secondary transfer term, excitation to the N = 0 level (e = 1) is considered. At the lowest pressure studied, 39 mTorr of N_2, $B_{ej} \geq N_e T_{ej}$ for $j \geq 6$, which means that half or more of the population in the states with $N \geq 3$ has come from multiple collision events.

Although the final solution of this kinetic equation for the T_{ej} requires an iterative technique, a by-product of which is the estimation of nearly all of the T_{ij}, three approximate methods have been tried to provide a simple solution. The three methods are similar in that they all assume a functional form of B_{ej} which allows direct fitting of the population ratios versus pressure to obtain the transfer rates; these differ in the form and complexity chosen. Two criteria are used to judge the validity of the rate constants so obtained: conformity to the qualitative observations; and a correct sum over final levels j, since $\sum_j T_{ej}$ should agree with the value $\overline{T}_e$ obtained from the analysis for total transfer rates. The first approximation, that of limiting slopes (see Fig. 6), yields transfer rates corresponding to the qualitative observations but the sums are a factor of two or three larger than the $\overline{T}_e$. A second assumption, that $B_e \propto P$, yields sums closer to $\overline{T}_e$. Finally, assuming (as in the determination of total rates) that B_e is a weighted average (and not a function of pressure) yields sums in even closer agreement. When the individual transfer rates are scaled by the ratio $\overline{T}_e$ (as determined in the last section) divided by $\sum_{j \neq e} T_{ej}$ (as determined via these assumptions on B_{ej}), good agreement is found among the three methods. The average of these initial estimates is then used as the starting poing for the iterative solutions.

A total of 210 individual T_{ij} are involved in the iterative procedure. Of these, 70 are available from the experimental data (5 different initially excited levels each relaxing into 14 others). Of the remaining 140 T_{ij}, over two-thirds are related to either the measured rates or one another by invoking detailed balancing, an assumption which is examined below. This leaves 45 independent T_{ij} whose values are estimated as follows. As mentioned previously, it is qualitatively found that the transfer rates vary smoothly with ΔN. Plots of the measured T_{ej} vs. various trial functions of ΔN show that upward transfer rates can be represented as

$$T_{ij} = g_j \exp (A_{\Delta ij} \Delta E_{ij} + F_{\Delta ij}) \qquad (7)$$

where g_j is the degeneracy of the final state $(2J'+1)$, ΔE_{ij} is the difference in energy of the initial and final states, and $A_{\Delta ij}$ and $F_{\Delta ij}$

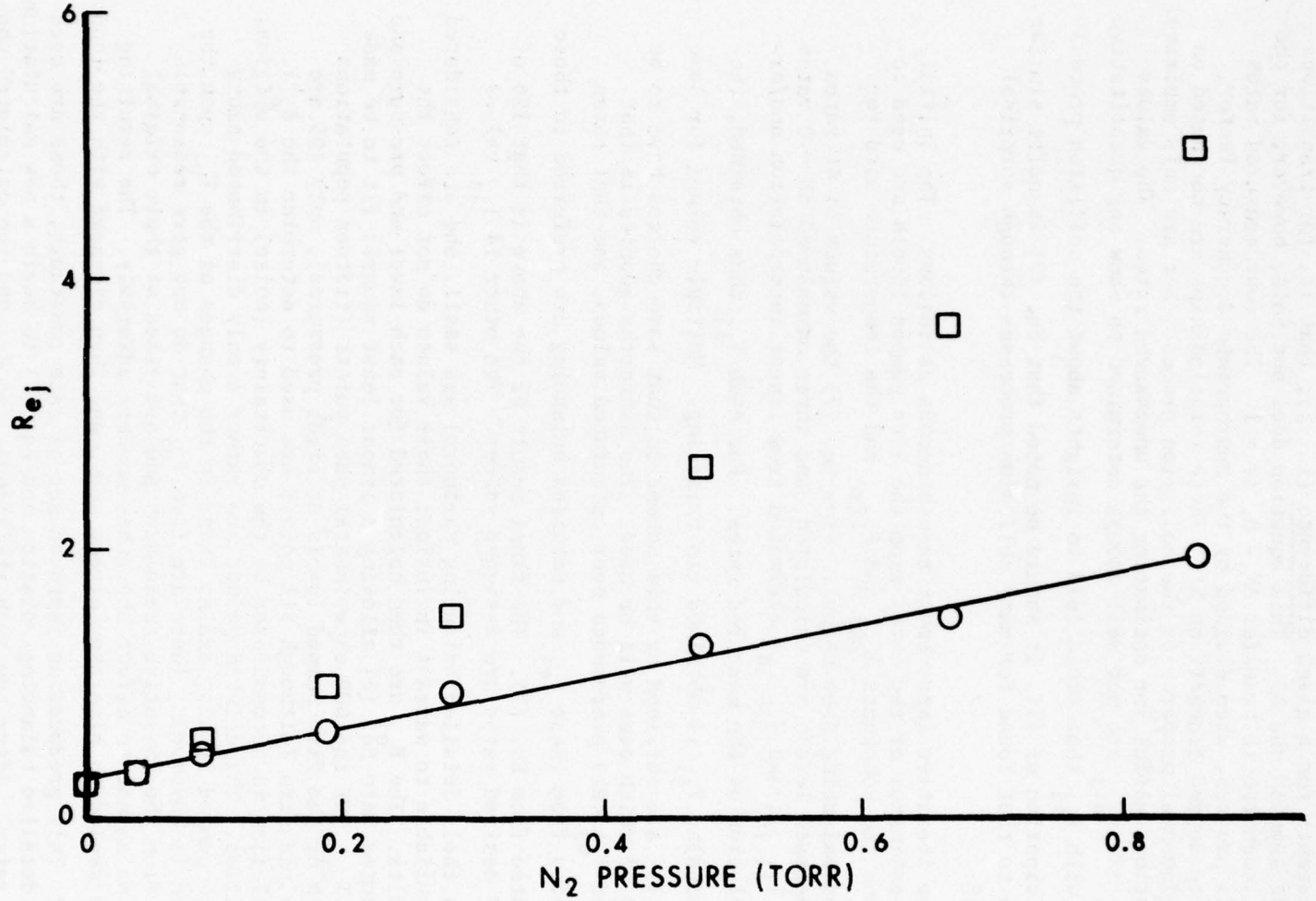

Figure 6. A plot of R_{ej} vs. pressure for the $F_1(3)$ (e = 7) initially pumped level transferring to the $F_1(2)$ (J = 5) level. Squares are uncorrected R_{ej}; circles represent final values of R_{ej} corrected for secondary transfer. Points at zero and 0.04 torr contain overlapping circles and squares.

are constants for a given difference (i - j); that is, for transitions with the same ΔN and ΔJ. This equation does not hold, however, for the nearly isoenergetic transfer $\Delta N = 0$, $\Delta J = 1$. The four measured rates for this process, when divided by the appropriate degeneracy factor, appear to depend linearly on N'. These relationships are not based on any fundamental property of the collision process, but are only empirical correlations useful for estimating the unmeasured rates. The values of $A_{\Delta ij}$ and $F_{\Delta ij}$ are not well enough determined to show any quantitative change with Δ_{ij} that could lead to insights about the collision process. In anticipation of III, it should be noted that Eq. (7) is quite similar in form to that found for many collision processes through surprisal analysis.

The iterative improvement then proceeds as follows. The initial, scaled estimates of the rates from the five pumped levels are used to determine the constants $A_{\Delta ij}$ and $F_{\Delta ij}$, and the temperature used for detailed balancing (see below). From Eq. (7) the values of 48 rates from unpumped levels are calculated, and three unmeasured $\Delta N = 0$ rates ($T_{5,4}$; $T_{11,10}$; and $T_{15,14}$) estimated from linear interpolation and/or extrapolation of the measured rates. For each T_{ij} thus obtained, the corresponding T_{ji} is obtained via balancing. Multiple values for some of the T_{ij} are obtained by this scheme so that some choices have to be made as to which ones will be used. The hierarchy adopted is that measured T_{ej} take preference over calculated values, and that rates calculated from these T_{ej} and detailed balancing are preferred to those calculated from Eq. (7). The final result of the above is that 196 of the 210 desired rates are assigned values. The other 14 T_{ij} values (7 plus their detailed balancing partners) are small, and are considered too unreliable to warrant inclusion; their values do not affect the final fits. The B_{ej} are then calculated for each level and pressure and substituted into Eq. (6) allowing a linear least squares fit to be made to the T_{ej}. Of the 600 experimental data points (fifteen populations for each of the five pumped levels at eight pressures), only 495 are used in the fits (although all points are used to determine the B_{ej}). This deletion is necessitated by the uncertainty (noise) in the original intensities. The deleted points are rather evenly distributed among the five pumped levels, and no trend in the changes of the T_{ej} upon the deletion is observed. There are five T_{ej} that do not give reasonable values from the iterative techniques and are fixed at their original values so as not to affect the other numbers adversely. The resulting T_{ej} are scaled to give the correct sums, and then averaged with the input values. This produces an improved set of rate constants; these are used in the detailed balancing relation and Eq. (7) to begin a new calculation of the rates. After ten such iterations, the T_{ej} and the calculated constants converged to within experimental error. The measured state-to-

state rotational transfer cross sections determined from the final, scaled values of the rates, along with the scaling factors, are presented in Table 3. The uncertainties quoted are one standard deviation as obtained from the least squares fits. The complete matrix of transition rates for N_2 collisions both measured and calculated, is given in Table 4 in units of per torr, per radiative lifetime. Even after the iterations are complete, the computed sums of the T_{ej} are still slightly different from the measured $\overline{T}_e$. The final quoted values are obtained by dividing the results of the final iteration by the scaling factor $\sum_{j \neq e} T_{ej}/\overline{T}_e$, which is a few percent different from unity (Table 3). The overall reliability of the T_{ij} will be addressed in the discussion section.

There are not enough data points to apply the above iterative procedure to the experimental results obtained with H_2 and Ar as collision partners, so a ratio technique similar to that used in the analysis of the total rotational transfer rates is employed. The initial estimates of the T_{ej} for these two fill gases (two pumped levels each) are divided by the corresponding rates for N_2 collisions and averaged to form an overall ratio for each of the two gases. The B_{ej} appropriate for H_2 and Ar are then calculated from these ratios and the transfer rates for collisions with N_2 (and the background gas; see Appendix II). The T_{ej} obtained from linear fits to Eq. (3) then provide improved ratios for the start of the next iteration. As with N_2, the sums of the individual rates do not sum to the corresponding total transfer rates and so are normalized after each iteration. The ratios obtained for transitions with large ΔN are unreliable (see uncertainties in Table 3) and are not used to find the average ratios during the iterations, but their inclusion does not appreciably alter these ratios. The iterations converge rapidly, after less than ten cycles, and provide the rotational transfer rates for collisions of A state OH with Ar and H_2 that are given in Table 5.

$R_2 3$ Excitation

All of the results discussed above are obtained from measurements in which the initially pumped level is an F_1 level. Two qualitative observations can be made from an examination of the raw data, and are borne out in the final state to state rate analysis. One of these, noted earlier, is the propensity for $F_1 \rightarrow F_1$ over $F_1 \rightarrow F_2$ for a given change of N; the second is the relatively small size of the nearly isoenergetic transfer $F_1 \rightarrow F_2$ within the initially pumped rotational level. Since these results appear to be general and may have mechanistic implications (see below and III) it is desirable to inquire as to the corresponding behavior observed when an F_2 level is excited. A clean excitation of an F_2 level was carried out by tuning to the $R_2 3$ absorption line (e = 8), and fluorescence scans were made with N_2 as the fill gas. The low line strength for $R_2 3$ made quantitative measurements unreliable. However,

TABLE 3. MEASURED ROTATIONAL TRANSFER CROSS SECTIONS $\sigma_{ij}(\text{Å}^2)$ FOR COLLISIONS OF OH WITH N_2.

i(N)	1(0)	3(1)	7(3)	9(4)	13(6)
j					
1	-	8.59±.27	3.57±.24	1.20±.08	0.50±.07
2	5.66±.90	4.08±.44	3.52±.59	0.59±.12	0.67±.16
3	15.99±.35	-	6.61±.39	4.59±.29	0.87±.30
4	3.75±.60	9.07±.54	4.33±.14	2.97±.18	2.27±.17
5	10.14±1.5	14.93±.30	10.22±.32	6.89±.74	2.23±.32
6	5.46±.49	2.25±.54	9.34±.46	5.22±.23	3.13±.42
7	2.50±.62	7.99±.42	-	10.57±.32	5.09±.34
8	1.92±.37	3.08±.33	4.11±.23	3.77±.42	3.49±.34
9	2.41±.30	3.30±.16	9.89±.36	-	4.81±.30
10	0.75±.08	1.29±.14	2.42±.17	2.51±.02	5.33±.73
11	2.35±.11	1.02±.23	2.41±.06	8.41±.14	9.80±.27
12	0.94±.06	1.03±.06	1.20±.04	1.46±.18	6.72±.33
13	0.59±.04	0.25±.18	0.84±.07	1.91±.16	-
14	0.61±.11	0.43±.03	0.68±.09	0.67±.09	3.27±.13
15	0.16±.02	0.39±.12	0.19±.08	2.02±.23	4.49±.30
Scaling Factor[a]	1.02	1.05	1.04	1.11	.88

[a]The ratio of the sum of the cross sections in each column to the total transfer cross section (Table 2) for that level.

TABLE 4. CALCULATED AND MEASURED ROTATIONAL TRANSFER RATES $T_{ij}(torr^{-1}\tau^{-1})$ FOR N_2.

i/j	1	2	3	4	5	6	7	8	9	10	11	12	13	14	15
1	-	1.02	2.88	.68	1.83	.98	.45	.35	.43	.14	.42	.17	.11	.11	.03
2	1.15	-	1.47	1.69	1.68	.99	1.42	.46	.19	.16	.29	-	.08	-	-
3	1.55	.74	-	1.64	2.69	.40	1.44	.56	.59	.23	.18	.18	.05	.08	.07
4	.48	1.07	2.06	-	1.94	1.64	1.10	.69	.59	.36	.34	.08	.18	-	-
5	.86	.71	2.27	1.30	-	1.06	1.73	.50	.92	.29	.43	.17	.12	-	-
6	.66	.59	.48	1.55	1.50	-	2.24	1.41	.98	.45	.45	.26	.23	.04	.13
7	.64	.64	1.19	.78	1.84	1.68	-	.74	1.78	.44	.43	.22	.15	.12	.04
8	.28	.33	.79	.78	.86	1.68	1.18	-	.85	1.13	.84	.28	.31	.19	.13
9	.22	.11	.83	.54	1.24	.94	1.91	.68	-	.45	1.52	.25	.34	.12	.36
10	.16	.16	.47	.58	.69	.76	1.00	1.62	.81	-	1.12	.88	.67	.17	.21
11	.40	.24	.31	.46	.86	.64	.83	1.01	2.26	.93	-	.53	1.02	.18	.19
12	.33	-	.64	.21	.68	.75	.83	.67	.74	1.47	1.07	-	1.41	.66	.45
13	.09	.12	.16	.41	.40	.57	.92	.63	.87	.96	1.77	1.21	-	.59	.81
14	.41	-	.52	-	-	.20	.91	.87	.70	.55	.72	1.28	1.33	-	1.74
15	.10	-	.41	-	-	.63	.23	.54	1.86	.60	.66	.76	1.60	1.53	-

TABLE 5. ROTATIONAL TRANSFER RATES ($torr^{-1}\ \tau^{-1}$) FOR COLLISIONS WITH H_2 and Ar

a. H_2			b. Ar		
j	T_{3j}	T_{7j}	j	T_{3j}	T_{9j}
1	1.04 ± .04	.51 ±.02	1	.60 ±.03	.06 ±.02
2	.72 ± .03	.11 ±.03	2	.44 ±.04	.05 ±.05
3	-	.79 ±.04	3	-	.18 ±.02
4	.79 ±.04	.50 ±.01	4	.44 ±.02	.22 ±.03
5	1.55 ±.03	1.27 ±.06	5	.86 ±.03	.19 ±.02
6	.33 ±.04	.79 ±.09	6	.23 ±.02	.23 ±.03
7	.86 ±.03	-	7	.29 ±.02	.45 ±.02
8	.40 ±.03	.39 ±.07	8	.093±.009	.55 ±.02
9	.44 ±.02	.93 ±.04	9	.20 ±.01	-
10	.13 ±.01	.24 ±.02	10	.093±.008	.27 ±.02
11	.09 ±.01	.44 ±.02	11	.040±.007	.51 ±.03
12	.08 ±.02	.22 ±.01	12	.015±.007	.13 ±.01
13	.08 ±.01	.11 ±.01	13	.033±.009	.15 ±.01
14	.056±.004	.03 ±.01	14	.018±.007	.045±.003
15	.04 ±.01	.20 ±.04	15	.008±.003	.07 ±.01

qualitative examination of the scans exhibiting rotationally transferred OH yields confirmation of the corresponding propensities, *viz.* $F_2 \rightarrow F_2$ is preferred over $F_2 \rightarrow F_1$, and transfer between the neighboring spin components of a given N (e.g., T_{67}) is relatively small. The trends exhibited in Table 4 for the fitted T_{ij}, although more reliable for transfer from F_1 levels, are in general accord with this single direct observation of an F_2 level undergoing transfer.

Detailed Balancing

The principle of detailed balancing, for a variety of kinetic processes, as done here, is often invoked to obtain unmeasured rates from measured ones. This states that, at thermal equilibrium, the forward and backward rate constants k_f and k_b for the processes $A + B \rightleftarrows C + D$ are related by

$$k_f/k_r = \frac{g_{C,D}}{g_{A,B}} \exp\left[-\left(E_{C,D} - E_{A,B}\right)/k\theta\right] \qquad (8)$$

where the g's are the degeneracies and E's are the energies of the respective collision partners; k is Boltzmann's constant and θ is the equilibrium temperature. Even if the system is not at full thermal equilibrium, the rates of isolated collision events must also obey this relationship (since the collision partners cannot 'know' they are not in equilibrium[25]), given that a suitable temperature (usually translational) can be defined.

Our measured rates for N_2 collisions provide 10 pairs of T_{ij} and T_{ji} for the processes

$$OH(i) + M \underset{T_{ji}}{\overset{T_{ij}}{\rightleftharpoons}} OH(j) + M$$

where the degeneracies and internal energies of the OH are well defined. What we actually obtain are the rates for the reactions

$$OH(i, \langle E_t \rangle) + M(\langle Q \rangle) \xrightarrow{T_{ij}} OH(J, \langle E_t' \rangle) + M(\langle Q' \rangle)$$

and

$$OH(j, \langle E_t \rangle) + M(\langle Q \rangle) \xrightarrow{T_{ji}} OH(i, \langle E_t'' \rangle) + M(\langle Q'' \rangle),$$

where the brackets denote averages that are not state specific with regard to the OH translational energy, E_t, or the internal energy Q of the collision partner M. If the ground state OH (from which OH(i) and OH(j) are formed by single photon absorption) is in rotational-translational thermal equilibrium, and if this equilibrium in E_t, as well as that in Q, is not disturbed by the collisional process, then Eq. (8) will hold.

The major difficulty arises from the internal energy part of Q; any strong propensity rules for the collision partner would upset the thermal equilibrium. However, the similarity between results for N_2 (high density of internal states) and for Ar (low density) suggests no such effects. We therefore consider it valid to examine our measured rates as an illustration of the detailed balancing principle.

In Fig. 7, these ten ratios are plotted logarithmically, and with error bars, vs. the energy difference. The ratios indeed show the expected behavior, and a straight line fit can be used to extract θ, the 'detailed balancing temperature.' The result is that θ = 420K, which is reasonable in view of the ground state rotational temperature (360K), the presumed temperature of the N_2 (room temperature = 300K), and our expectations concerning $\langle E_t \rangle$ and $\langle Q \rangle$. This value of θ is used to form the detailed balancing relationships between other pairs of T_{ij} and T_{ji} necessary for the iterative solutions.

Detailed balancing is an important principle, widely used but seldom directly examined experimentally for single collision events. We find the results exhibited in Fig. 7 comforting, in that they demonstrate detailed balancing over a wide range of energy and degeneracy differences within a single collision system.

DISCUSSION

Reliability of the Results

The manner in which the rate constants for transfer are obtained from the measured fluorescent intensities precludes a quantitative analysis of errors. We have identified several 'direct' sources of error affecting the $\overline{T}_e$ values in the experimental data and parameters used. These are the intensities, the pressures, the lifetime, the correct temperature, the quenching rates, and the fitting error. This last is simply the confidence limits in the parameters obtained from the regression techniques. A quenching rate uncertainty of 10% will lead to about a 5% uncertainty in the absolute transfer rates. Combining all these 'direct' sources of error as independent leads to an estimate of the uncertainty in the measured $\overline{T}_e$ of about 10%. This does not, however, take into account errors arising through the analysis scheme, which we feel are impossible to judge.

The relative values of the state-to-state rate constants must be viewed differently. Of the above contributions to the uncertainty in $\overline{T}_e$, only the fitting errors are important here. However, there are obviously correlations among the T_{ij} and their associated uncertainties. The rates out of the initially pumped levels, the T_{ej}, are better determined than the unmeasured rates; some gauge of their self-consistency can be obtained from the detailed balancing plot, Fig. 7. As for

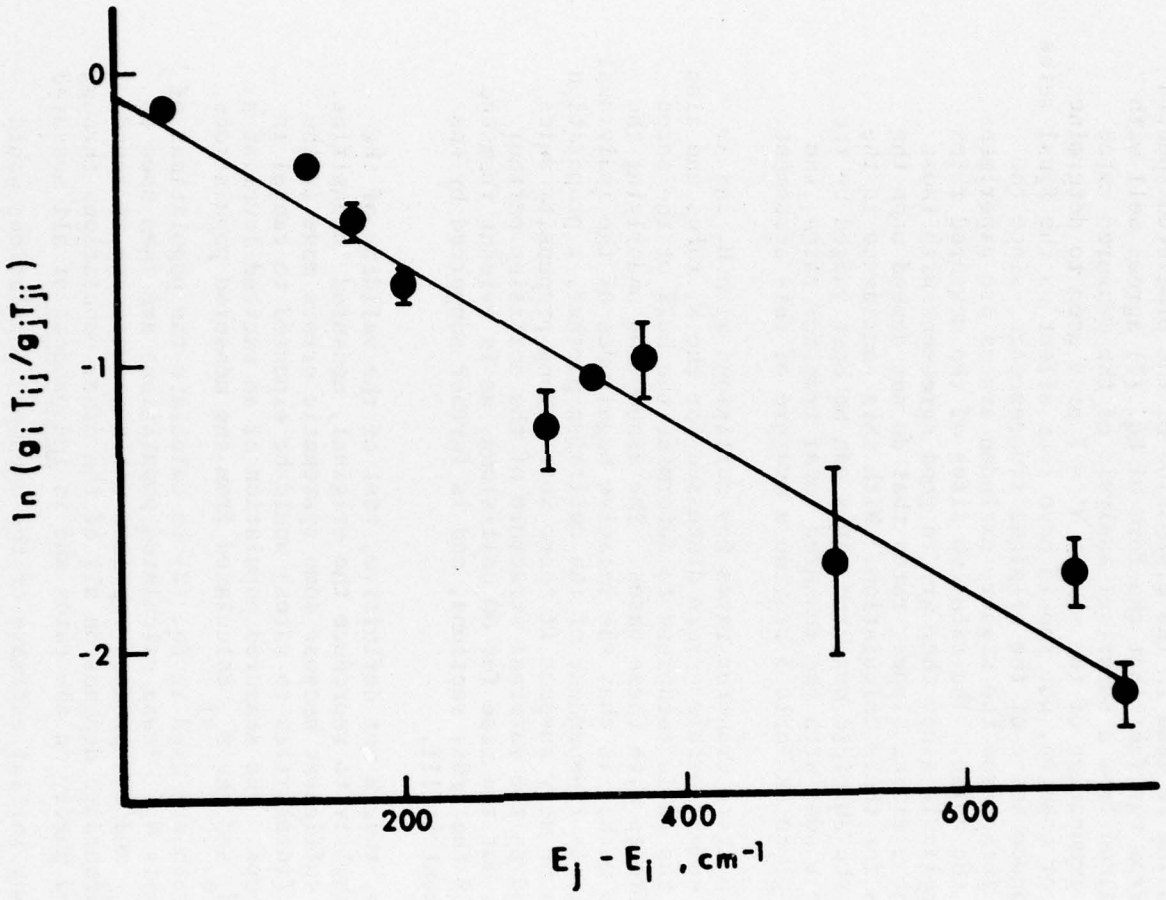

Figure 7. Ratio of directly measured forward and backward rates, corrected for degeneracy vs. energy difference. These should yield a straight line if detailed balancing is applicable; the line drawn is an unweighted least-squares fit. Error bars are from confidence limits on the iterative fit; when not shown, they are smaller than the circles plotted.

the unmeasured rates, while a comparison of any given pair could be misleading, the relatively smooth trends exhibited over the entire matrix permit conclusions as to propensities.

The greatest source of possible systematic error in the state-to-state rates, with N_2 as a collision partner, is the calculation of the unmeasured rates, particularly those from the F_2 levels. That this is not a severe problem is seen in the discussion of the predicted spectra below and also from the fact that the form of Eq. (7) agrees well with the results obtained from a surprisal analysis of the measured rates (see III). The truncation of the sum at N' = 7 or 8 used to determine the B_{ej} is also of concern, but should have less effect on the final rates than does the random noise of the original fluorescence, since the intensities resulting from the higher, excluded states are experimentally less than the noise. The relative sizes of the measured rates are considered reliable since they are in good agreement with those obtained from the limiting slopes, rates that do not depend upon the unmeasured rates for their calculation. With this confidence in the relative rates, the absolute measured rates can be best judged by the agreement of their sums with the measured total transfer rates; the scaling factors given in Table 3 provide a measure of this agreement.

The state-to-state transfer rates for collisions with H_2 and Ar suffer from the same possible errors discussed for the N_2 rates and also from the use of the ratio technique to determine the bulk of the secondary transfer effects with these gases. The assumption underlying the use of the ratio method is that the relative magnitudes of the individual rates are relatively independent of the collision partner, a proposition that would again be very suspect if there were strong propensity rules that could depend on the internal structure of the collision partner. However, this is not the case for OH collisions, as is evident from the relative sizes of the cross sections, and is further supported by the surprisal treatment in III.

A necessary, though not definitive, test of the validity of the rates is their ability to reproduce the original, measured intensities. The test is not sufficient because some systematic errors made in the forward process (intensities to rates) would be expected to cancel in the reverse process. The measured population of an excited level at a given pressure N_e and the B_{ej} calculated from the measured populations of the other levels are used in Eq. (2) to calculate the populations of the unpumped levels N_j. These calculated populations are then used to determine new B_{ej} and the process repeated until convergence is found. This iterative procedure depends on all of the other populations through the B_{ej}, is based purely on the rates and is <u>independent</u> of all measured populations. (Any initial estimate of the unpumped populations would give the same final calculated populations; the use of the measured populations simply gives faster convergence.) These populations, the

measured N_e and the N_i calculated from them, are used to predict the intensities of the thirty-two line fluorescence spectra. The intensities are normalized to the total in the band. An example of the spectrum predicted in this way is given in Table 1 and shown in Fig. 4, and the overall error is calculated in an RMS fashion, since the normalization used demands that the sum of the deviations equal zero. Although some of the lines are found to have a 10-12% deviation, the RMS error is always less than 4%, and is typically in the range of 1-2%, for all excited levels and N_2 pressures studied.

As mentioned above, the signal to noise ratio for these excitations makes the populations obtained from them of dubious value for rate measurements; however, they do provide a check on the calculated rates and particularly on the assumption that F_1 levels and F_2 levels behave similarly in the collision process. When the calculated and observed spectra for these excitations are compared, the RMS deviations are less than 5% and usually two to three percent, quite comparable to those obtained from the five well studied excitations. Again it should be emphasized that the calculated spectra are determined directly from the rate constants and do not depend on any measured populations. Due to the propensity for spin conservation, the calculated R_23 spectra depend heavily on the approximate F_2 to F_2 and F_2 to F_1 rates, so the conformity of the measured and calculated line intensities is directly supportive of similar transfer behavior for the F_1 and F_2 levels.

Other Investigations

There are few data appearing in the literature on rotational transfer in $A^2\Sigma^+$ OH, and none that may be directly compared with the results obtained here. Carrington[30] selectively excited the $F_2(11)$ level in a low pressure acetylene-oxygen flame using atomic line excitation; the total rate $\overline{T}_{22}$ due to all the flame gases is in the range 3-10 $torr^{-1}\tau^{-1}$, which is compatible with our results.

Two studies have exploited the fact that high rotational levels of $A^2\Sigma^+$ OH are produced in the photodissociation of H_2O by krypton resonance radiation. Kaneko, Mori, and Tanaka[31] report total transfer rates out of the N' = 20 level of 8.0 $torr^{-1}\ \tau^{-1}$ for H_2 and 1.9 $torr^{-1}\ \tau^{-1}$ for N_2. The rates for collisions with H_2 are in good agreement with the values reported here. Their N_2 transfer rate, however, is a factor of five lower than given here. While there is a small apparent fall off of

[30] T. Carrington, "Rotational Transfer in the Fluorescence Spectrum of OH ($^2\Sigma^+$)," J. Chem. Phys. 31, 1418-1419 (1959).

[31] M. Kaneko, Y. Mori, and I. Tanaka, "Electronic Quenching and the Rotational Relaxation Rate of OH* ($^2\Sigma^+$) Produced by the Vacuum-ultraviolet Decomposition of Water," J. Chem. Phys. 48, 4468-4473 (1968).

the rate with increasing N' (see Table 2), this decrease would not appear to be rapid enough to resolve the discrepancy. The lack of details given in their paper makes any attempt at reconciliation of these values speculative at best. Kley and Welge[32] report relative rates for $\Delta N = -1$ transitions for the levels N' = 9 -20, obtained from modelling their results on the photodissociation. Their rates vary exponentially as E_{ij}/kT, where it is assumed that they used a temperature of near 300 K. The results presented here show less variation with energy, but the disagreement is understandable since they do not include the effects of the degeneracy, the contribution of collision transitions with $\Delta N \neq -1$, or the effects of secondary collisions, all of which have been shown to be of importance.

Elastic Reorientation

Hanle effect measurements establish coherence, or definite phase relationships, among excited state m_J levels via absorption of polarized and/or directional light.[23] The Hanle effect, collisional broadening rate for a single initially excited level, together with rates for rotational transfer and quenching, provide a rate of coherence destruction during elastic collisions. The rate of elastic reorientation of the angular momentum vector is 12% larger than the rate of destruction of the "alignment," the type of coherence produced by linearly polarized excitation.[33]

A Hanle effect broadening rate has been measured[23] for the $F_1(N=1)$ level in collisions with H_2. In that study, however, the fluorescence was not resolved, so that it included contributions from levels populated by rotational energy transfer from $F_1(1)$. Since a rotational transfer collision does not necessarily destroy the coherence, the apparent broadening rates measured in such an experiment can be less than the broadening rate for the initially excited level alone.[22]

We have made Hanle effect observations on the A-state.[21,34] Measurements were made of the change in fluorescence polarized perpendicular to an applied magnetic field, when the field is switched from zero to a value corresponding to complete magnetic depolarization. The fluorescent signals were rotationally resolved in order to separately determine the degree of polarization of the light emitted by the initially excited level, and of the light emitted by those levels populated by energy transfer in the presence of a given pressure of collision partner.

---

[32] D. Kley and K. H. Welge, "Quenching and Rotational Relaxation of OH ($A^2\Sigma^+$, v'=0,K')," J. Chem. Phys. 49, 2870-2871 (1968).

[33] P. R. Berman and W. E. Lamb, Jr., "Influence of Foreign Gas and Resonant Collisions on Line Shapes," Phys. Rev. 187, 221-266 (1969).

[34] R. K. Lengel and D. R. Crosley, unpublished data.

We could observe no polarization in levels populated by either rotational or vibrational energy transfer (which we consider as supportive of a long-lived collision picture; see below). Noise considerations place the upper limit of degree of polarization in these transferred levels as < 3%. Since full retention of coherence in a rotational energy transfer collision would lead to a polarization > 40%, we conclude that there is no appreciable retention of the coherence. Thus we take the measured, rotationally unresolved broadening rate[23] as the broadening rate for the initially pumped level alone. That rate, *viz.*,12.7 $torr^{-1}$ τ^{-1}, with our $\overline{T}_e$ and Q, and the 1.12 ratio, yields a rate of elastic reorientation of 4.7 $torr^{-1}$ τ^{-1}, corresponding to a cross section of 11 $Å^2$.

Summary and Mechanistic Implications

The most accurate but least detailed information about rotational transfer is given by the total transfer rates $\overline{T}_e$. They are considered accurate in that they are little dependent on the approximations concerning secondary transfer, but lack the detail of true state-to-state rates. They do show that there is only a weak dependence of the rotational transfer on initial level and that the structureless Ar is more efficient as a collision partner than diatomic H_2. This lack of internal state dependence is not surprising in view of the fact that even the most exoergic transfer studied directly, OH(N'=6) → OH(N'=0), provides only five open rotational channels in the H_2. The N_2 cross sections are larger than those of Ar, but the data are inconclusive as to whether this is due to the density of internal states of the nitrogen. The state-to-state rotational rates suffer from some loss of accuracy due to secondary collision effects, but do provide some detailed information. For transitions where $\Delta N = \Delta J$, there are no propensities for particular ΔN changes but rather a smooth variation with energy defect. For example, when the final state degeneracies are included, the measured rate for the single quantum transfer N'=6 → N'=5 is actually less than the rate for the isoenergetic, multiquantum process N'=3 → N'=0. There is, however, a propensity for spin conservation; transitions with $\Delta N = \Delta J$ are faster than the corresponding ones with $\Delta N \neq \Delta J$.

We have earlier[2] hypothesized that the vibrational energy transfer occurs via a long-lived, closely coupled collision; further observation of details of that process continues to encourage (though not prove) that view, which is discussed in II and III. A long-lived collision provides fewer implications for rotational transfer. However, the relatively large size of the cross sections, and the lack of any strong propensities for ΔN, are at least compatible with a long-lived or close-coupling mechanism. The surprisal analysis results (III) better quantify the trends in the T_{ij} and lend further support to this picture.

ACKNOWLEDGEMENT

We gratefully acknowledge the National Science Foundation for their support of the portion of this work carried out while both authors were at the University of Wisconsin.

REFERENCES

1. R. N. Zare and P. J. Dagdigian, "Tunable Laser Fluorescence Method for Product State Analysis," Science 185, 739-747 (1974).

2. R. K. Lengel and D. R. Crosley, "Rotational Dependence of Vibrational Relaxation in $A^2\Sigma^+$ OH," Chem. Phys. Lett. 32, 261-264 (1975).

3. S. Green, "Dipole Moment and Hyperfine Constants of OD $A^2\Sigma^+$ from ab initio Calculations," J. Chem. Phys. 58, 4327-4330 (1973).

4. W. H. Henneker and H. E. Popkie, "Theoretical Electronic Transition Probabilities in Diatomic Molecules. I. Hydrides," J. Chem. Phys. 54, 1763-1778 (1971); B. Liu, "Accurate Theoretical Oscillator Strengths for Diatomic Molecules, CH and OH," Symposium on Molecular Structure and Spectroscopy, Columbus, Ohio, June 1975, Paper RF 14.

5. C. H. Chen and M. G. Payne, "A Potential Hydroxyl Ultraviolet Laser," Opt. Comm. 18, 476-478 (1976).

6. M. J. Berry, "Laser Studies of Gas Phase Chemical Reaction Dynamics," Ann. Rev. Phys. Chem. 26, 259-280 (1975); J. H. Birely and J. L. Lyman, "Effect of Vibrational Reagent Energy on Measured Reaction Rate Constants," J. Photochem. 4, 269-280 (1975).

7. H. Levy, "Photochemistry of the Troposphere," Adv. Photochem. 9, 369-524 (1974).

8. M. Nicolet, "An Overview of Aeronomic Processes in the Stratosphere and Mesosphere," Can. J. Chem. 52, 1381-1396 (1974).

9. F. Kaufman and F. P. Del Greco, "Formation, Lifetime and Decay of OH Radicals in Discharge Flow Systems," J. Chem. Phys. 35, 1895 (1961).

10. G. H. Dieke and H. M. Crosswhite, "The Ultraviolet Bands of OH," John Hopkins University Bumblebee Report No. 87 (1948), republished in J. Quant. Spectry. Radiat. Transfer 2, 97-199 (1963).

11. R. K. Lengel and D. R. Crosley, Energy Transfer in $A^2\Sigma^+$ OH. II. Vibrational," to be published (referred to as II).

12. R. K. Lengel and D. R. Crosley, "Energy Transfer in $A^2\Sigma^+$ OH. III. Surprisal Analysis," to be published (referred to as III).

13. R. D. Levine and R. B. Bernstein, "Energy Disposal and Energy Consumption in Elementary Chemical Reactions: the Information Theoretic Approach," Acct. Chem. Res. 7, 393-400 (1974).

14. R. K. Lengel, "Energy Transfer in $A^2\Sigma$ OH," Ph.D. Thesis, University of Wisconsin, Madison, WI, June 1976.

15. M. A. A. Clyne and S. Down, "Kinetic Behaviour of OH $X^2\Pi$ and $A^2\Sigma^+$ Using Molecular Resonance Fluorescence Spectrometry," J. Chem. Soc. Far. Trans. II 70, 253-266 (1974).

16. A. McKinzie, M. F. R. Mulcahy and J. R. Steven, "Reaction Between Hydrogen Atoms and Nitrogen Dioxide," J. Chem. Soc. Far. Trans. I 70, 549-559 (1974).

17. W. E. Wilson, "A Critical Review of the Gas-Phase Reaction Kinetics of the Hydroxyl Radical," J. Phys. Chem. Ref. Data 1, 535-572 (1972).

18. J. A. Silver, W. L. Dimpfl, J. H. Brophy and J. L. Kinsey, "Laser-induced Fluorescence Determination of Internal-state Distribution of OH Produced by H + NO_2 in Crossed Molecular Beams," J. Chem. Phys. 65, 1811-1822 (1976) H. Haberland, P. Rowher and K. S. Schmidt, "Reactive Scattering of H and D Atoms. II. Isotope Effect on the Angular Distribution of H,D and NO_2," Chem. Phys. 5, 298-305 (1974); J. C. Polanyi and J. J. Sloan, "Detailed Rate Constants for the Reactions Atomic Hydrogen + Ozone → Hydroxyl (v'J') + Molecular Oxygen, and Atomic Hydrogen + Nitrogen Dioxide → Hydroxyl (v'J') + Nitrogen Monoxide," Int. J. Chem. Kinet. 7, (Symp 1), 51-60 (1975).

19. D. R. Crosley and R. K. Lengel, "Relative Transition Probabilities and the Electronic Transition Moment in the A-X System of OH," J. Quant. Spect. Rad. Transfer 15, 579-591 (1975).

20. L. Klein, "Strengths of the Rotational Lines of OH ($A^2\Sigma$ - $X^2\Pi$) and Occupation of the Molecular Energy Levels in Arc Plasmas," J. Quant. Spect. Rad. Transfer 13, 581 (1973).

21. D. R. Crosley, ""Level Crossings and Anisotropic Emission in a $^2\Sigma$ - $^2\Pi$ Transition," BRL Report, to be published.

22. T. A. Caughey and D. R. Crosley, "Coherence Retention During Rotationally Inelastic Collisions of Selectively Excited Diatomic Sulfur," Chem. Phys. 20, 467-475 (1977).

23. K. R. German, T. H. Bergemann, E. M. Weinstock and R. N. Zare, "Zero-field Level Crossing and Optical Radio-frequency Double Resonance Studies of the $A^2\Sigma^+$ States of OH and OD," J. Chem. Phys. 58, 4304-4318 (1973).

24. D. R. Crosley and R. K. Lengel, "Relative Transition Probabilities in the A-X System of OD," J. Quant. Spect. Radiat. Transfer 17, 59-71 (1977).

25. J. I. Steinfeld and W. Klemperer, "Energy Transfer Processes in Monochromatically Excited Iodine Molecules. I. Experimental Results," J. Chem. Phys. 42, 3475-3497 (1965).

26. R. K. Lengel and D. R. Crosley, "Comment on 'Electronic Quenching and Vibrational Relaxation of the OH($A^2\Sigma^+$, v'=1) State'," J. Chem. Phys. 64, 3900-3901 (1976).

27. K. R. German, "Direct Measurement of the Radiative Lifetimes of the $A^2\Sigma^+$ (v=0) States of OH and OD," J. Chem. Phys. 62, 2584 (1975).

28. J. H. Brophy, J. A. Silver, and J. L. Kinsey, "Direct Measurement of the Radiative Lifetime of the $A^2\Sigma^+$ (v'=0, K'=1, J'=3/2) State of OH and OD," Chem. Phys. Lett. 28, 418-421 (1974).

29. W. L. Dimpfl, private communication (1976).

30. T. Carrington, "Rotational Transfer in the Fluorescence Spectrum of OH ($^2\Sigma^+$)," J. Chem. Phys. 31, 1418-1419 (1959).

31. M. Kaneko, Y. Mori, and I. Tanaka, "Electronic Quenching and the Rotational Relaxation Rate of OH* ($^2\Sigma^+$) Produced by the Vacuum-ultraviolet Decomposition of Water," J. Chem. Phys. 48, 4468-4473 (1968).

32. D. Kley and K. H. Welge, "Quenching and Rotational Relaxation of OH ($A^2\Sigma^+$, v'=0,K')," J. Chem. Phys. 49, 2870-2871 (1968).

33. P. R. Berman and W. E. Lamb, Jr., "Influence of Foreign Gas and Resonant Collisions on Line Shapes," Phys. Rev. 187, 221-266 (1969).

34. R. K. Lengel and D. R. Crosley, unpublished data.

APPENDIX I. INTEGRATED SIGNALS

We here demonstrate the equivalence of the population ratios in the steady-state approach, and the ratios of the fully integrated signals $S_j = \int_0^\infty N_j \, dt$. The population N_j, for $j \neq e$, is given by

$$\frac{dN_j}{dt} = N_e \, T_{ej} P + \sum_{i \neq e} N_i \, T_{ij} P - N_j \, D_j$$

where $D_j = 1 + P(Q + \sum_i T_{ji})$. Application of the steady-state approximation (Eq. (2)) for all $j \neq e$ in the n-level system, yields n - 1 equations for the n - 1 ratios N_j/N_e.

We examine the actual time dependence under delta-function excitation conditions, i.e., $N_e(0) = A$, and $N_j(0) = 0$ for all $j \neq e$. Integrating the above equation over all time yields

$$\int_0^\infty \frac{dN_j}{dt} \, dt = S_e \, T_{ej} \, P + \sum_{i \neq e} S_i \, T_{ij} \, P - S_j \, D_j$$

But $\int_0^\infty \frac{dN_j}{dt} \, dt = N_j(\infty) - N_j(0) = 0$ if $j \neq e$. Consequently the ratios S_j/S_e obey the same equations as do the steady-state population ratios N_j/N_e. The population N_e or the integrated signal S_e must of course be non-zero for the experiment to exist, so that use of the ratios is valid.

APPENDIX II. BACKGROUND TRANSFER

The effects of collisions with the background gases H_2O and NO_2 cannot be ignored in the actual analysis (see Fig. 3) as they are in the simplified steady state equations. While in the vibrational transfer studies[2,11] they are simply subtracted, the iterative procedure used for the rotational transfer demands their explicit inclusion, since they contribute to the secondary collision corrections. We examine these necessary corrections within the framework of the steady-state equations. The starting point, Eq. (2), properly reads

$$N_e(T_{ej}\,P + C_{ej}) + \sum_{i\neq e} N_i(T_{ij}\,P + C_{ij})$$

$$= N_j\left\{1 + P(Q + \sum_i T_{ji}) + \sum_i C_{ji}\right\},$$

where the C_{ij} is the background-gases counterpart to $T_{ij}P$ (the background gases are always at the same pressure). Eq. (4) is actually

$$R_e = \overline{T}_e P + \overline{C}_e - \sum_{j\neq e} (T_{je}P + C_{je})\,\frac{N_j}{N_e}\ ,$$

where $\overline{C}_e$ is like $\overline{T}_e$. The term $\sum_{j\neq e} C_{je}\,N_j$ is found experimentally to be negligible, and is dropped from the analysis. For consideration of the state-to-state rates, however, the situation is more complicated, since the background transfer rates enter into the <u>form</u> of $B_{ej}(P)$. Here,

$$R_{ej} = H_j N_j / N_e = T_{ej}p + C_{ej} + B_{ej}(P)/N_e$$

where B_{ej} is now a function of P:

$$B_{ej}(P) = \sum_{i\neq e} N_i\,(T_{ij}P + C_{ij})$$

and $$H_j = 1 + \overline{C}_j + (Q + \overline{T}_j)P.$$

Since it is found that the relative magnitudes of the T_{ij} are quite independent of collision partner for the fill gases studied, we assume this is true for the background gases as well. Hence we take $C_{ij} = c\,T_{ij}$, where c is a constant determined using zero fill-gas-pressure runs. We then replace $T_{ij}P + C_{ij}$ by $T_{ij}(P + c)$ in the above expression for $B_{ej}(P)$. For further information, see Ref. 14.

DISTRIBUTION LIST

No. of Copies	Organization
12	Commander Defense Documentation Center ATTN: DDC-TCA Cameron Station Alexandria, VA 22314
1	Commander US Army Materiel Development and Readiness Command ATTN: DRCDMA-ST 5001 Eisenhower Avenue Alexandria, VA 22333
1	Commander US Army Aviation Research and Development Command ATTN: DRSAV-E 12th and Spruce Streets St. Louis, MO 63166
1	Director US Army Air Mobility Research and Development Laboratory Ames Research Center Moffett Field, CA 94035
1	Commander US Army Electronics Command ATTN: DRSEL-RD Fort Monmouth, NJ 07703
1	Commander US Army Missile Research and Development Command ATTN: DRDMI-R Redstone Arsenal, AL 35809
1	Commander US Army Tank Automotive Research & Development Cmd ATTN: DRDTA-RWL Warren, MI 48090
1	Commander US Army Armament Materiel Readiness Command ATTN: DRSAR-LEP-L, Tech Lib Rock Island, IL 61201
3	Commander US Army Armament Research and Development Command ATTN: DRDAR-LC Dr. J. Lannon Dr. R. Field Dr. L. Harris Dover, NJ 07801
1	Commander US Army Harry Diamond Labs ATTN: DRXDO-TI 2800 Powder Mill Road Adelphi, MD 20783
1	Director US Army TRADOC Systems Analysis Activity ATTN: ATAA-SL, Tech Lib White Sands Missile Range NM 88002
1	Stanford University Department of Chemistry ATTN: Dr. P. K. Lengel Stanford, CA 94305
	Aberdeen Proving Ground
	Marine Corps Ln Ofc Dir, USAMSAA